FINAL REPORT

Project O2

March 2020

Macroscopic Fundamental Diagram Approach to Traffic Flow with Autonomous/Connected Vehicles

Dr. Robert W. Whalin | Jackson State University

Guojing Hu, Ph.D. Candidate | Jackson State University

STRIDE | Southeastern Transportation Research, Innovation, Development and Education Center

UF | Transportation Institute UNIVERSITY of FLORIDA

TECHNICAL REPORT DOCUMENTATION PAGE

1. Report No. Project O2	2. Government Accession No.	3. Recipient's Catalog No.
4. Title and Subtitle Macroscopic Fundamental Diagram Approach to Traffic Flow with Autonomous/Connected Vehicles		**5. Report Date** March 2020 **6. Performing Organization Code**
7. Author(s) Dr. Robert Whalin, Jackson State University Guojing Hu, Doctoral Candidate, Jackson State University		**8. Performing Organization Report No.** STRIDE Project O2
9. Performing Organization Name and Address Jackson State University 1400 John R. Lynch Street Jackson, MS 39217		**10. Work Unit No.** **11. Contract or Grant No.** Funding Agreement Number 69A3551747104
12. Sponsoring Agency Name and Address University of Florida Transportation Institute Southeastern Transportation Research, Innovation, Development and Education Center 365 Weil Hall, P.O. Box 116580 Gainesville, FL 32611 U.S Department of Transportation/Office of Research, Development & Tech 1200 New Jersey Avenue, SE Washington, DC 20590 United States		**13. Type of Report and Period Covered** 9/1/2018 to 3/25/2021 **14. Sponsoring Agency Code**

15. Supplementary Notes

16. Abstract

Connected and autonomous vehicles (CAVs) have the capability to acquire real-time information from each other while human-driven vehicles (HVs) are standalone in the vehicle roadway navigation system. The information asymmetry poses great challenges in managing and controlling vehicles in the mixed traffic. To address such challenges, a new lane-changing algorithm is proposed for CAV platoons to bypass a relatively slow HV. The simulation results indicate that, at all the CAV penetration levels, the proposed lane-changing algorithm provides significant performance improvements to the whole mixed traffic flow, in terms of outflow and travel time.In addition, how and when the benefits associated with CAVs will start to impact the performance of urban network is a question of interest for traffic operators. This study proposes an analytical capacity model for mixed urban corridors based on the concept of macroscopic fundamental diagram (MFD). The model incorporates not only the full spectrum of CAV penetration rates, but also reaction time of different vehicle types resulted from different CAV technologies. Numerical experiments verify that different reaction time settings yield disparate results. As CAV penetration rates increased, the urban street capacity may increase or decrease depending upon the reaction time settings. Finally, the concept of MFD is adopted as an index to evaluate the traffic network capacity and further appraise the quality of discrete network design problem (DNDP). This study formulates a bi-level programming model where in the lower level, traffic flows are assigned to the newly extended network subject to user equilibrium theory, and the upper level determines which links should be added to achieve the maximum network capacity. Finally, the methodology is implemented in a test network and the simulation results verify the capacity benefit of using the MFD-based method to solve the NDP under stochastic OD demands. Specifically, capacity paradox is also presented in the test results.

17. Key Words	18. Distribution Statement
connected, autonomous vehicles, traffic flow, optimization, traffic control, traffic simulation	No restrictions

19. Security Classif. (of this report)	20. Security Classif. (of this page)	21. No. of Pages	22. Price
		58 Pages	

DISCLAIMER

The contents of this report reflect the views of the authors, who are responsible for the facts and the accuracy of the information presented herein. This document is disseminated in the interest of information exchange. The report is funded, partially or entirely, by a grant from the U.S. Department of Transportation's University Transportation Centers Program. However, the U.S. Government assumes no liability for the contents or use thereof.

ACKNOWLEDGEMENT OF SPONSORSHIP AND STAKEHOLDERS

This work was sponsored by a contract from the Southeastern Transportation Research, Innovation, Development and Education Center (STRIDE), a Regional University Transportation Center sponsored by a grant from the U.S. Department of Transportation's University Transportation Centers Program.

Funding Agreement Number - 69A3551747104

LIST OF AUTHORS

Lead PI:

Robert W. Whalin, Ph.D., P.E.
Jackson State University
robert.w.whalin@jsums.edu
ORCID 0000-0002-8712-9434

Additional Researchers:

Guojing Hu, Ph.D. Candidate
Jackson State University
guojinghu.jsu@gmail.com

TABLE OF CONTENTS

LIST OF FIGURES

LIST OF TABLES

ABSTRACT

Connected and autonomous vehicles (CAVs) have the capability to acquire real-time information from each other while human-driven vehicles (HVs) are standalone in the vehicle roadway navigation system. The information asymmetry poses great challenges in managing and controlling vehicles in the mixed traffic. To address such challenges, a new lane-changing algorithm is proposed for CAV platoons to bypass a relatively slow HV. The simulation results indicate that, at all the CAV penetration levels, the proposed lane-changing algorithm provides significant performance improvements to the whole mixed traffic flow, in terms of outflow and travel time.

In addition, how and when the benefits associated with CAVs will start to impact the performance of urban network is a question of interest for traffic operators. This study proposes an analytical capacity model for mixed urban corridors based on the concept of macroscopic fundamental diagram (MFD). The model incorporates not only the full spectrum of CAV penetration rates, but also reaction time of different vehicle types resulted from different CAV technologies. Numerical experiments verify that different reaction time settings yield disparate results. As CAV penetration rates increased, the urban street capacity may increase or decrease depending upon the reaction time settings.

Finally, the concept of MFD is adopted as an index to evaluate the traffic network capacity and further appraise the quality of discrete network design problem (DNDP). This study formulates a bi-level programming model where in the lower level, traffic flows are assigned to the newly extended network subject to user equilibrium theory, and the upper level determines which links should be added to achieve the maximum network capacity. Finally, the methodology is implemented in a test network and the simulation results verify the capacity benefit of using the MFD-based method to solve the NDP under stochastic OD demands. Specifically, capacity paradox is also presented in the test results.

EXECUTIVE SUMMARY

With the development of automation and connectivity technology, there will be more connected and autonomous vehicles (CAVs) entering the road network. Before all the existing human-driven vehicles (HVs) are replaced by CAVs, there will be a long transition period that CAVs and HVs are mixed on the roadway. Originally, equipped with vehicle-to-vehicle communication capability, CAVs are expected to improve the road capacity due to smaller reaction times and headways. However, in the mixed traffic, the movement of human-driven vehicles are uncertain and unpredictable, which will severely hinder the communication between CAVs. How to manage the operation of CAVs in the mixed traffic is a challenge. To address this problem, the study proposed a lane-changing algorithm to guide CAV platoons to bypass the slower HVs. The simulation in a 2-kilometer freeway verified that the proposed algorithm speeds up not only the CAVs but also the HVs, the total travel time decreased, and the highway outflow was improved.

In addition, how the mixed traffic would affect the road capacity is still on debate. Most studies, through the simulation tools, proved the positive impact of CAVs on road capacity. However, in recent years, some research, through the theoretical analysis, reminded the readers that the more CAVs may not always increase the highway capacity. Motivated by this finding, the study was devoted to an analytical methodology to examine how the urban street capacity would evolve with the introduction of CAVs. The numerical experiments found that the urban street capacity was not only related to the penetration rate of CAVs, but also influenced by the reaction time of different vehicle following types. The improvement of capacity becomes obvious when the CAV penetration rate is over 60%. But if the reaction times of different vehicle following types are improperly set, more CAVs entering the urban street may decrease the capacity, especially when the CAV penetration rate is low.

The advent of CAVs also has the potential to stimulate vehicle travel demand by improving road capacity, reducing travel and parking cost. Especially for those who are too young or old to drive, their travel demands can be met in the era of CAVs. However, to what extent the travel demand will be increased is still uncertain, different studies yield different conclusions. For example, it was stated that CAVs would add 20% or more demand for new vehicle-miles traveled *(1)*, another saying was that automated vehicles would increase daily trip amount by 4.14% on average *(2)*. The aroused travel demand uncertainty makes it challenging to determine how to modify existing road networks to improve travel flow/throughput. To circumvent this challenge, the study implements the concept of macroscopic fundamental diagram (MFD) identify design solutions that would improve the transportation network. Through a test network simulation, the proposed method is verified to yield robust network design solutions.

CHAPTER 1. A Lane Change Algorithm for Mixed Human and Connected Autonomous Traffic

1.1 INTRODUCTION

With the introduction of connected and autonomous vehicles (CAVs), the roadway system is ushering in a phase of mixed traffic where CAVs coexist with HVs. Because of the potential impact on many aspects related to road transportation, e.g. traffic congestion, energy consumption, travel delays, road capacity and safety, the mixed stage has attracted more and more attention from researchers, vehicle manufacturers and policymakers. Replacing all human-driven vehicles (HVs) on the entire road network with CAVs will significantly increase the highway capacity, due to smaller time headways between consecutive CAVs. However, the transition from HVs to full CAVs is still a long way off. In the transition period, how the mixed traffic containing both HVs and CAVs affects the system performance of a traffic network is a problem worth studying. With HVs whose speed and acceleration information cannot be acquired by CAVs, the traffic throughput and stability will be largely affected by the highly random and uncertain movements of HVs. One of the efficient manners to reduce the interference of HVs is the dedicated lane separating CAVs from HVs, which exerts a great impact on both road capacity and safety. However, dedicated lane use is an expensive strategy and only suitable when the CAV penetration reaches to a certain degree *(3,4,5).* Another alternative is CAV platooning, where platoons of CAVs closely follow a leading vehicle. Because of the closer spacing, it is expected that the road capacity can be improved as a result of the higher traffic density, and the cooperative behavior of CAVs within a platoon *(6).* By all indications, when the CAV penetration is at a relatively low level, allocating a dedicated lane for CAVs is wasteful and may incur traffic congestion in regular lanes. In order to improve the flow efficiency of mixed traffic, a well-developed platooning and lane-changing management protocol is necessary to arrange operations of two different types of vehicles.

Toward this objective, a cooperative adaptive cruise control (CACC) framework for CAV car-following and lane-changing in a mixed traffic environment is developed in this study. This study makes the following contributions. First, the headway time of CAVs is incorporated into the Intelligent Driver Model (IDM) to model CAV's acceleration behavior. Second, a lane-changing algorithm for CAV platoons to bypass HVs is proposed, so as to improve travel efficiency for CAVs without sacrificing the speed of HVs. Third, through the simulation experiment based upon VISSIM and COM interface using Python coding, the proposed CACC framework is tested and proved to reduce the system travel time and improve the freeway outflow.

1.2 OBJECTIVE

- Model driver behaviors of CAVs.
- Propose a lane-changing algorithm for CAV platoons to interact with HVs.
- Evaluate the highway operation performance of the lane-changing algorithm.

1.3 LITERATURE REVIEW

Traditional car-following models, suitable for human driving, are unable to capture all possible driver behaviors in the mixed traffic environment. The most commonly used model for the car-following behaviors of CAVs is the intelligent driver model (IDM) developed by Treiber, Hennecke and Helbing *(7).* IDM is an adaptive cruise control (ACC) system intended for adjusting the driver's longitudinal desired velocity and safety time gap *(8).* By incorporating the wireless Vehicle-to-Vehicle (V2V) communication technology, ACC is extended to the cooperative adaptive cruise control (CACC) system, which handles both longitudinal and lateral spacing controls for CAVs. CACC could access richer information from surrounding vehicles, enabling vehicles in a platoon to maintain a smaller headway compared to ACC *(9).* For example, Zhao and Sun *(10)* set 1.4s as the minimum desired headway of ACC while 0.5s for CACC. The IDM was leveraged to model the connected environment with active V2V communications *(11,12,13).* In addition to the car-following behavior for longitudinal control, lane-changing decision-making as lateral control is also a vital component in the CACC system. Lane changing is considered as one of the most challenging driving maneuvers to understand and to predict, and the corresponding driving decisions are often seen as a major source of congestion and collisions *(14).* Although CAVs are able to receive accurate information from neighboring CAVs through the V2V technology, HVs cannot be perceived and their movements usually involve high levels of uncertainty and randomness, which often impair the performance of traffic control developed for pure CAVs. Therefore, it is important to carefully consider how the traffic flow should be controlled within the context of mixed CAVs and HVs.

To address the challenge of mixed traffic flow, many studies resort to CAV platooning strategy. However, through the analytical formulation of Markov chain model, Ghiasi et al. *(15)* revealed that, under the mixed traffic circumstance, CAV platooning may not always help improve highway capacity. If the sum of HV following HV and CAV following CAV headway time is larger than twice of HV following CAV headway time, vehicle platooning intensity has a negative impact on traffic capacity. Furthermore, several simulation experiments also found that CAV platooning and platoon size have little effect on the mixed traffic capacity *(10,16).* It may be reasonable that under a mixed traffic environment, the interference of HVs, to some extent, limits CAVs' driving efficiency and throughput, even if a platooning scheme is applied. How to take full advantage of CACC technology and improve travel efficiency for the mixed traffic flow is still a challenge to be studied. Until now, there are very few studies focusing on the lane change problem in a mixed environment. Shi et al. *(16)* introduced a partial CAV lane change (PAL) for low CAV penetrations and full CAV lane change (FAL) for high CAV penetrations. Liu et al. *(17)* introduced an anticipatory lane change criterion to depict the interactions among CAVs and HVs, with which a quadratic increase of pipeline capacity to CAV penetration is obtained. Motivated by the research scarcity in mixed traffic flow, this study seeks to develop a new lane-changing algorithm to deal with the interactions between CAVs and HVs under various CAV penetrations. In this algorithm, the CAV platoon is allowed to change lanes in the form of sub-platoon.

In this study, we first put some effort into building an IDM to distinguish CAV following behaviors from those of HVs. Second, an innovative lane-changing algorithm is proposed for CAVs within a platoon to change lanes simultaneously in a mixed traffic environment when approaching an HV. The lane-changing algorithm aims to maximize the CAV driving efficiency through bypassing HVs. Third, several evaluation indicators are introduced to measure the performance of the proposed bypassing algorithm. Finally, based on the comparison of simulation results in a two-lane freeway, the lane-changing is tested to be an efficient strategy to improve the overall system performance of the mixed traffic environment under different CAV penetration levels, especially to reduce CAV travel time.

1.4 MICROSCOPIC MODEL FOR CAVS IN MIXED TRAFFIC

1.4.1 CAV Following Behaviors

For CAVs, the commonly used collision-free model - Intelligent Driver Model (IDM) is employed to describe the acceleration and deceleration behaviors *(7).* IDM is a microscopic model for examining traffic behavior on an individual level with emphasis on the relation to an ahead vehicle. The dependence on the speed difference between the vehicle and an ahead vehicle makes IDM collision-free, the expression of IDM acceleration/deceleration is shown in Equation (1).

$$IDM\_ac_u = a\left[1 - \left(\frac{v_u}{v_0}\right)^{\delta} - \left(\frac{s^*(v_u,\Delta v_u)}{\Delta x_u - l}\right)^2\right] \quad \text{Eq. (1)}$$

$$s^*(v_u,\Delta v_u) = s_0 + \max\left(0, v_u h + \frac{v_u \cdot \Delta v_u}{2\sqrt{ab}}\right) \quad \text{Eq. (2)}$$

In Equation (1), $\left(\frac{v_u}{v_0}\right)^{\delta}$ ensures a positive acceleration for vehicle u when its velocity is below the desired speed, otherwise a negative acceleration. $\frac{s^*(v_u,\Delta v_u)}{\Delta x_u - l}$ is designed to preclude crashes by forcing vehicle u with a preceding gap $(\Delta x_u - l)$ shorter than the desired gap $s^*(v_u,\Delta v_u)$ to decelerate. In Equation (2), s_0 is the jam between-vehicle spacing, which is only active in stationary traffic; $v_u h$ corresponds to the distance that vehicle u travels before responding to any changes of its preceding vehicle; $\frac{v_u \cdot \Delta v_u}{2\sqrt{ab}}$, designed to stabilize the platoon in terms of vehicle speed, is positive only when the current speed of vehicle u is larger than that of the preceding vehicle. The notations and values used in this study in Equations (1) and (2) are listed in Table 1 to depict car-following behaviors of CAVs *(17,18)*.

Table 1. Notations and Values Used in This Study for IDM

Notation	Explanation	Value used in this study for CAVs
a	Maximum acceleration	2 m/s2
b	Maximum deceleration	3 m/s2
l	Vehicle length	4 m
s_0	Jam spacing	2 m
v_0	Desired speed	30 m/s

h	Headway time	0.5 s
δ	Acceleration exponent	4
v_u	The current speed of vehicle u	
Δx_u	The bumper-to-bumper distance of vehicle u to the preceding vehicle	
Δv_u	Speed difference of vehicle u with the preceding vehicle	
$s^*(v_u, \Delta v_u)$	The desired distance of vehicle u from the preceding vehicle	
IDM_ac_u	Acceleration of vehicle u	

1.4.2 Innovative Lane Change Algorithm for CAVs

The most important innovation of the study is the development of a lane change algorithm for CAVs to bypass a preceding HV, therefore we also call it bypassing algorithm. An algorithm-based lane changing model is developed to guide the interactions between CAVs and HVs. The basic idea is that when a CAV platoon approaches an HV, the CAV platoon splits into sub-platoons seeking a longer distance from the preceding vehicle in another lane, so that changing to another lane (also called target lane) allows the sub-platoon to travel in a higher speed. Besides, if there's either a shorter space from the preceding vehicle in another lane, or the distance from the latter vehicle in another lane doesn't meet the safe distance, no lane-change will occur. Figure 1 is drawn to show the framework intuitively.

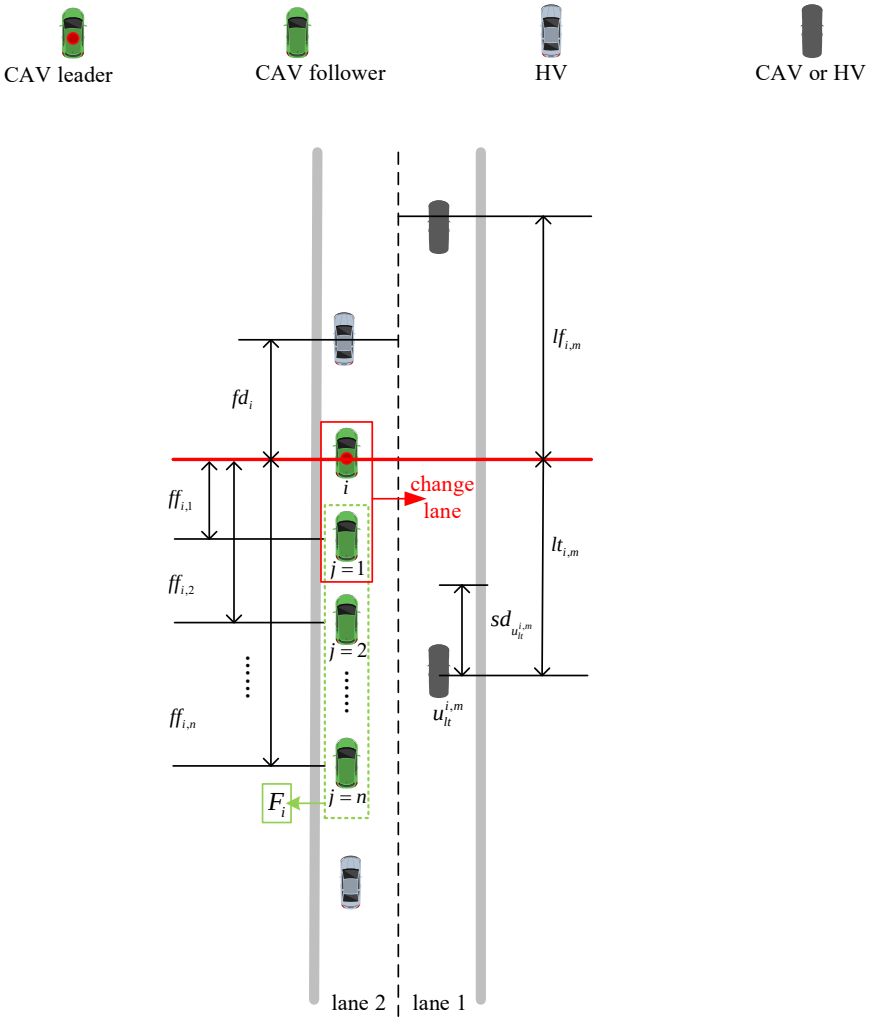

Figure 1. Lane-changing Operations of a CAV Platoon.

There are generally two scenarios in lane-changing operations of a CAV platoon.

(1) The first CAV i, acting as the platoon leader, accelerates until the desired speed is achieved, if the distance from leader i to the preceding HV (fd_i) is larger than both of the safety distance of leader i (sd_i) and the longitudinal distance to the front vehicle in another lane ($lf_{i,m}$). As the leader accelerates, each of the followers ($j = 1,2,\dots,n$ belonging to the CAV follower set F_i) maintains a dynamic response to the preceding vehicle, yielding a close following distance within the CAV platoon. The accelerations for the CAV leader and followers are modeled by the IDM.

(2) When the CAV platoon leader i approaches a preceding CAV in the current lane, the CAVs can form a larger platoon. However, if the preceding vehicle is an HV, and there is more forward space in another lane, then a split operation of the CAV platoon is triggered. Ideally, the maximum CAV sub-platoon seeks to change lanes when the safety distance of the following vehicle ($lf_{i,m}$) in the target lane permits. As Figure 1 shows, vehicle i leads a CAV platoon ($j = 1,2,\dots,n$) getting closer to an HV in lane 2, if the forward gap in the target lane ($lf_{i,m}, m = 1$) is

larger than that in the current lane (fd_i), and the backward gap in the target lane ($lf_{i,m}, m = 1$) allows the addition of two vehicles without breaching the safety distance required for the following vehicle ($sd_{u_{lt}^{i,m}}$), then vehicle i and vehicle $j = 1$ as a sub-platoon will simultaneously change to the target lane (lane 1), and vehicle $j = 2$ then becomes the new leader of the remaining sub-platoon ($j = 2,3, \dots, n$) in the original lane.

1.5 RESULTS

1.5.1 PTV VISSIM

The capability of the proposed modeling framework is demonstrated in a two-lane freeway, which is a 2-kilometer segment created in PTV VISSIM simulation. VISSIM is a microscopic road traffic simulator based on the individual behavior of vehicles. The goal of the microscopic modeling approach is the accurate description of traffic dynamics. Thus, the simulated traffic network can be analyzed in detail *(20)*. The simulator uses the so-called psycho-physical driver behavior model developed originally by Wiedemann (1974, 1999) *(19).* VISSIM is widely used for diverse problems by traffic engineers in practice as well as by researchers for developments related to road traffic. VISSIM offers a user-friendly graphical interface (GUI) through of which one can design the geometry of any type of road networks and set up simulations in a simple way. However, for several problems the GUI is not satisfying, for example, when the user aims to access and manipulate VISSIM objects during the simulation dynamically. For this end, an additional interface is offered based on the Component Object Model (COM) which is a technology to enable inter-process communication between software. The VISSIM-COM interface defines a hierarchical model in which the functions and parameters of the simulator originally provided by the GUI can be manipulated by programming. It can be programmed in any type of languages which is able to handle COM objects (e.g. Delphi, C++, Visual Basic, Java, Python and MATLAB, etc.). Through VISSIM-COM the user is able to manipulate the attributes of most of the internal objects dynamically *(20)*.

To dynamically control the inflows, increase CAV penetration rates, and manipulate the car-following as well as lane-changing behaviors of CAVs, the VISSIM-COM interface programmed in Python is implemented in this study. During simulation, VISSIM and Python communicate with each other via the COM interface of VISSIM. With the COM interface, Python has access to all the traffic data inside VISSIM, and controls driver behaviors of CAVs. Although the HV information (e.g. location and speed) in VISSIM platform can be obtained and the HV behaviors can be changed through COM, to be more realistic, we only control the CAV driving behaviors during the simulation process.

1.5.2 Simulation Settings

The detailed car-following, lane-changing models and the corresponding parameters for CAVs have been described in the previous section.

For HVs, the psychological-physiological Wiedemann 99 model *(19)* is employed to describe HV following behaviors. The concept of the Wiedemann model is that a fast-moving HV approaching

a slower preceding vehicle will start to decelerate once reaching its own individual safety perception threshold. Then, the speed may become smaller than the lead vehicle as a result of the driver's imperfection in the estimation of the lead vehicle speed *(21)*. Due to disparate physical characteristics, each HV has different perception thresholds of safety distance, desired speed and speed difference *(22)*. The Wiedemann car-following model is preset in VISSIM, and the default values are used in this study to model HV following behaviors. For example, at a given speed v(m/s), the safety spacing distance dx_safe is calculated by the equation $dx\_safe = d_0 + h \cdot v$ where the desired standstill distance between two HVs (d_0) is set as 1.5m, and the headway time h is 0.9s. Furthermore, the longitudinal oscillation for HVs is expected to be 4m, speed difference during the "following" state ranges from -0.35 to 0.35. The lane-changing behaviors of HVs are also described by the preset strategies in VISSIM: free lane changing and necessary lane changing. When the desired safety distance to the trailing vehicle on the target lane is satisfied, free lane changing is allowed for an HV to reach its desired speed through bypassing slower vehicles. Necessary lane changing happens when an HV is going to reach the next waypoint on its route. The default lane changing parameters in VISSIM are used to model the aggressiveness of lateral maneuvers for HVs.

1.5.3 Demonstration of Bypassing Algorithm

On the VISSIM simulation platform, the vehicle type, location, time, lane position and following distance of each vehicle are collected in real-time. Using the same simulation seed, the vehicle track and lane-changing behaviors are depicted in Figures 2 and 3 under input flow of 1500 vehicles per hour (veh/h).

Figure 2 demonstrates CAV and HV tracks with and without the CAV bypassing Algorithm. In the absence of CAV bypassing algorithm, CAVs adopt the same lane change rules as HVs. As seen in Figure 2(a), most of the CAV position-time curves with the bypassing algorithm are steeper than those without the bypassing algorithm. It is obvious that with the bypassing strategy the moving speeds of CAVs become faster, and interestingly, the speeds of HVs are slightly increased as well, as shown in Figure 2(b). The bypassing strategy is designed only for CAVs, no matter whether with or without the bypassing strategy, the driver behavior models of HVs are the same. A possible reason to explain the improvement of HV speeds is that in the mixed environment, not only HVs influence CAVs, but CAVs affect HVs as well. When a preceding CAV moves faster, the following HV will have a larger following distance which allows a higher acceleration. Therefore, the proposed CAV bypassing algorithm is shown to not only benefit CAVs, but also HVs in terms of travel speed.

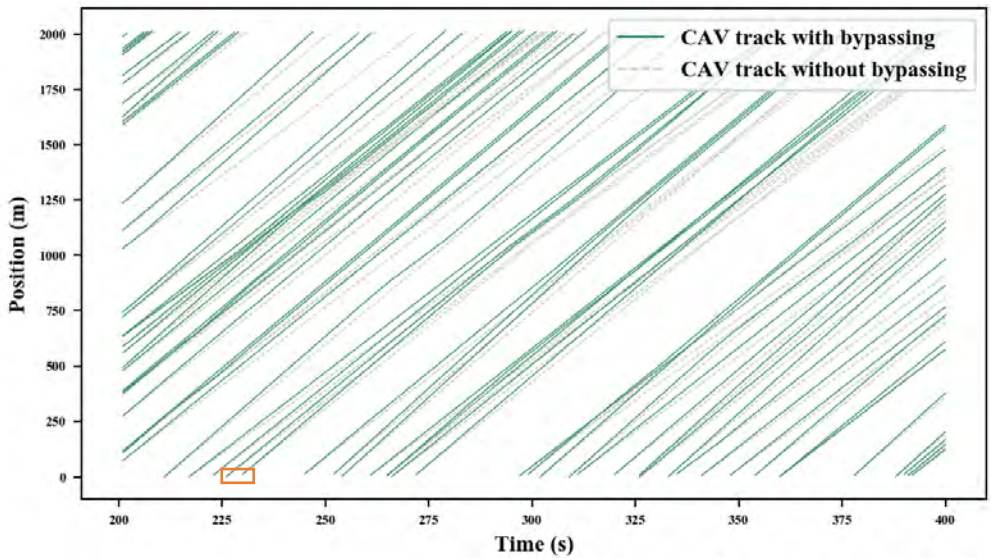

(a)

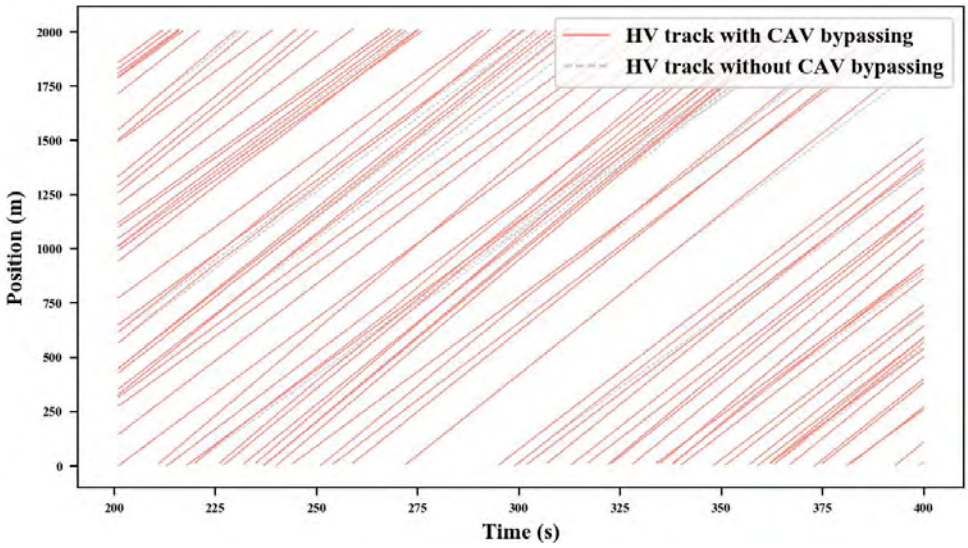

(b)

Figure 2. Track Comparison of (a) CAVs and (b) HVs with and without Bypassing Algorithm.

The simulation duration time in the case study is set at 3600 seconds to process all the vehicles. For visualization, we show the time series from 200 seconds to 400 seconds. Figure 3 exhibits the lane positions of CAV IDs from 24 to 163 over the time range 200 - 400 seconds. A CAV ID in the y-axis is the unique key for each vehicle determined in the order of input time in VISSIM. For example, the CAV of ID 24 is input to the simulated freeway prior to that of ID 25. In addition, the blank space in y-axis means HVs. For instance, vehicles of IDs 100, 99 and 98 are HVs, but vehicles of IDs 97 and 95 are CAVs. We can see from Figure 3 that the CAVs with bypassing strategy experience more lane changings than those without bypassing strategy. Compared to Figure 3(a), most of the CAVs in Figure 3(b) keep in the same lanes within the observed 200 seconds.

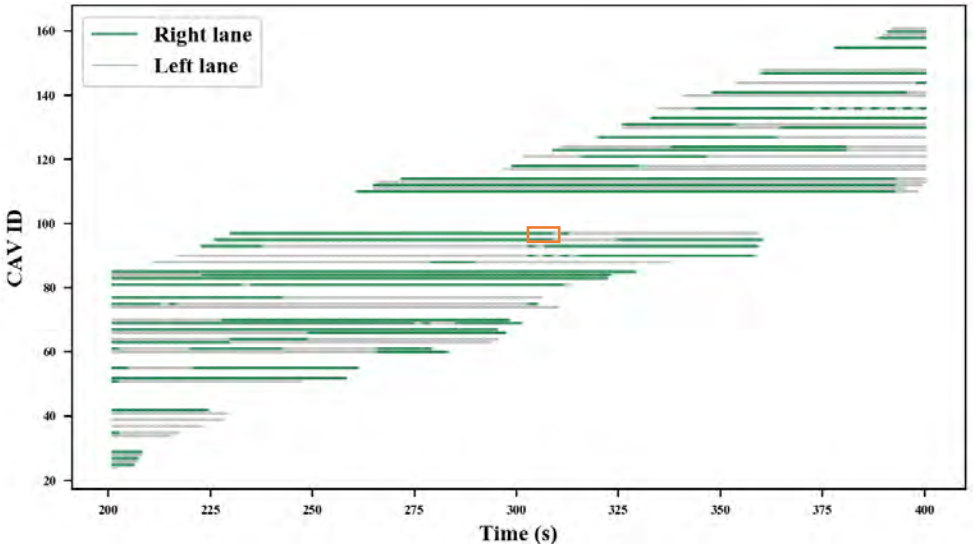

(a)

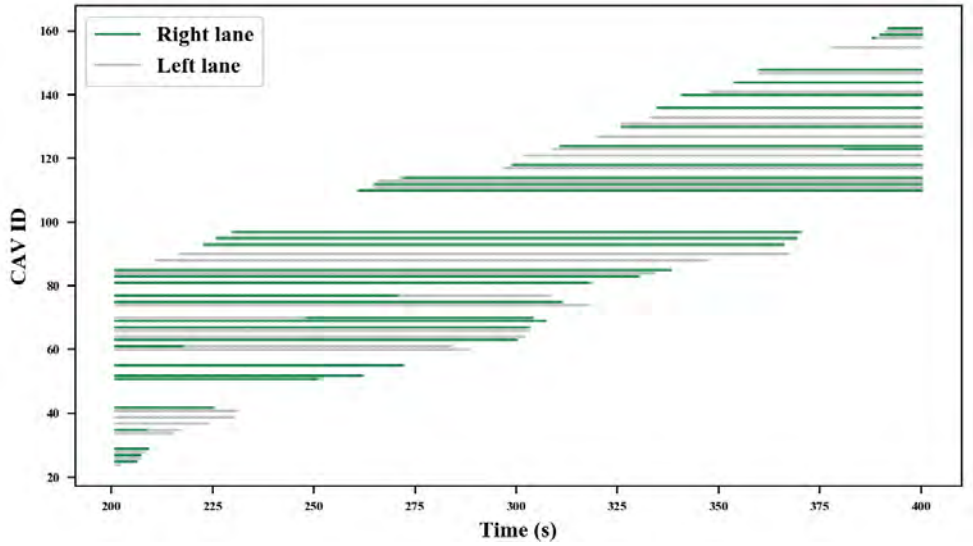

(b)

Figure 3. Comparison of CAV Lane Changing Behaviors (a) with bypassing (b) without bypassing.

Relating Figure 3(a) with Figure 2(a), in the orange boxes, CAVs with IDs 95 and 97 are input to the freeway at time 226 seconds and 230 seconds respectively. CAV 97 moves forward at a slightly higher speed to approach CAV 95 until a grouping platoon with the preceding CAV 97. Then, the CAV platoon of size 2 changes from the right lane to the left lane at the same time (309 seconds). After 2 seconds at time 311 seconds, the CAV platoon split, only CAV 97 changes lanes by itself. This phenomenon coincides with the behaviors proposed by the bypassing algorithm, with which CAVs form platoons when approaching, split into sub-platoons to bypass HVs and the sub-platoon could change lanes simultaneously.

Figure 4 shows the car-following distance of each CAV with and without the bypassing algorithm, which is in accordance with the lane-changing behaviors in Figure 3. For example, in Figure 3(a), CAV 117 travels on the left lane while CAV 118 moves on the right lane until time 330 seconds, CAV 118 makes a lane change to the left lane in front of CAV 117. This lane-changing behavior is also reflected in Figure 4(a), where before time 330 seconds, CAV 118 follows a vehicle in a small distance and CAV 117 has a large space in front, however, after changing lanes, CAV 118 gains a much longer following distance while CAV 117 follows closely behind CAV 118. It is not difficult to find that, compared to Figure 4(b) in which each CAV keeps a relatively single following distance, there are more gradient colors in Figure 4(a). The comparison result suggests that, with the bypassing strategy, CAVs travel in a more flexible manner, changing lanes according to the following distance.

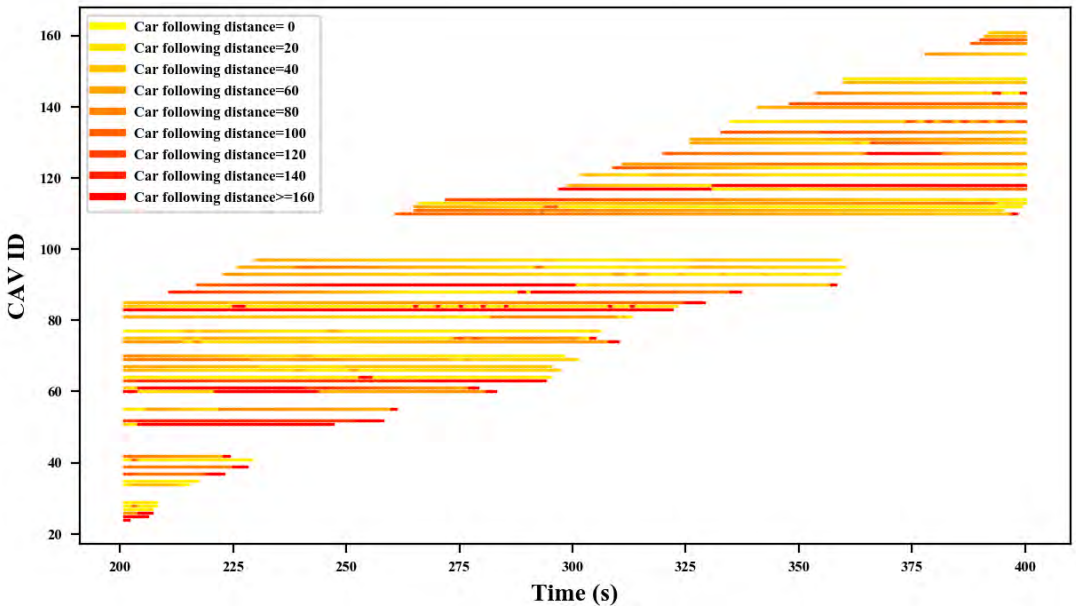

(a)

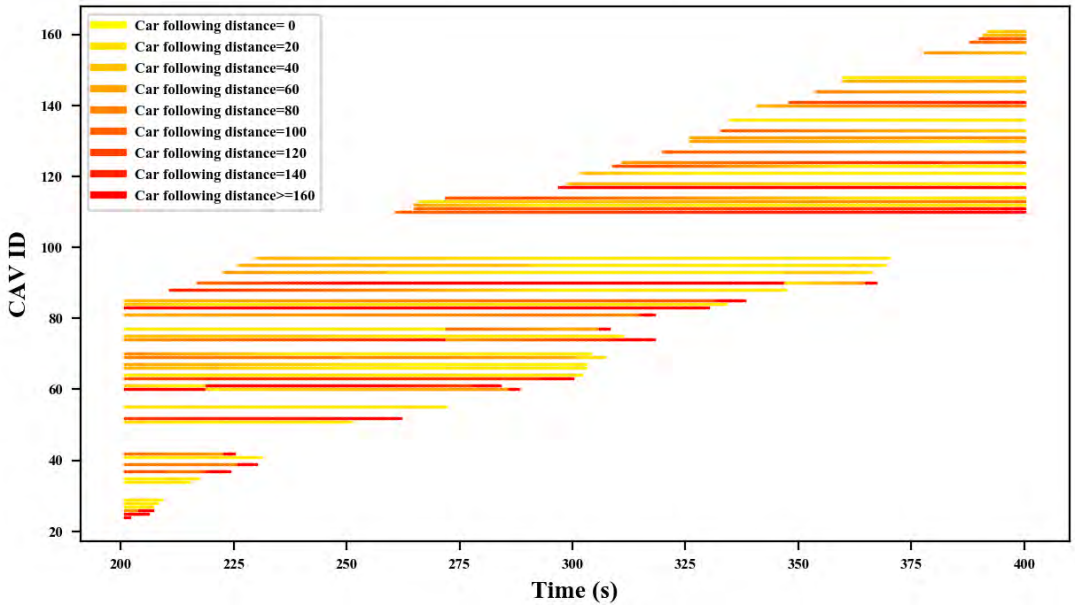

(b)

Figure 4. Comparison of CAV Car Following Distance (a) with bypassing (b) without bypassing.

1.5.4 Comparison of Traffic Evaluation Indexes

To test the performance of the presented controlling algorithm under different travel demands, the input volume increases from 500 veh/h to 3500 veh/h with an increment of 500 veh/h. Different CAV penetration rates are also considered in the study, increasing from 0% to 100%, with an increment of 10%. The 0% penetration indicates full of HVs on the freeway and 100% means all the vehicles on the road are CAVs. The characteristics of the mixed traffic flow are analyzed under different CAV penetrations and input flows. Furthermore, three different random seeds are implemented in simulations.

(1) Traffic Outflow

A detector is set up at the end of the 2-kilometer freeway to collect the outflow information in every 200 seconds. The outflows under a variety of input volumes ranging from 500 veh/h to 3500 veh/h are compared to capture the effectiveness of the proposed CAV controlling strategy. From the result shown in Figure 5, it is worth noting that, under low input flows, there is very little distinction drawn between the outflow with and without the bypassing lane-changing strategy. This phenomenon may be linked to the reason that the low input volumes have not reached the two-lane freeway capacity, so that all of the input vehicles can be discharged without latency. However, as inflow continues to increase from 1500 veh/h, the superiority of the bypassing algorithm is becoming more and more obvious. We thus conclude that the proposed bypassing algorithm exhibits the superiority in outflow, especially when the input flow reaches a high value, e.g. 3500 veh/h. In addition, in regard to freeway outflow, no matter how the CAV penetration changes, the proposed bypassing strategy outperforms the default controlling

algorithms in VISSIM. Figure 5 also reveals an overall growing tendency, with the bypassing algorithm, of the freeway outflow as CAV penetration rate increases, while increment of CAV penetration makes little difference to the freeway outflow without the bypassing algorithm. Therefore, without the bypassing algorithm, the CAV technology does not work in improving the freeway outflow.

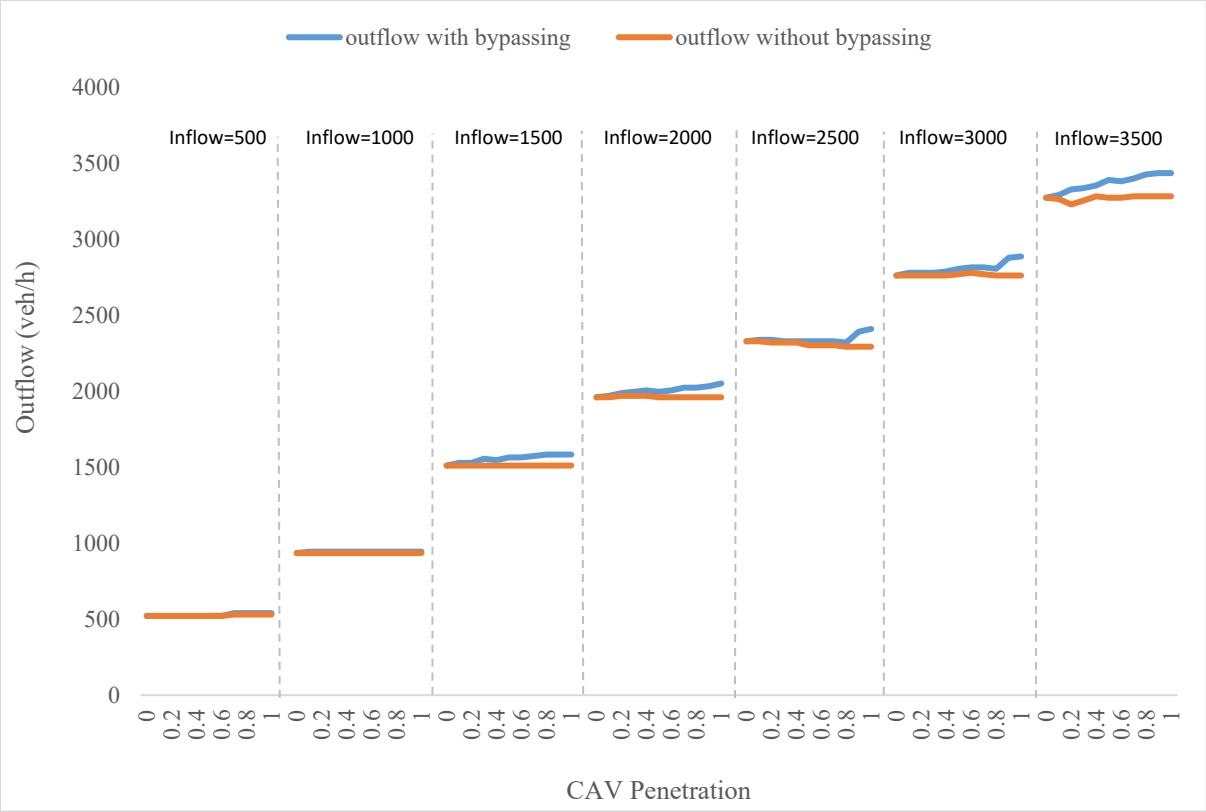

Figure 5. Outflow Under Different Input Volumes and Different CAV Penetrations.

(2) Travel Time

As Figure 6 shows, without the bypassing strategy, CAV penetration shows an insignificant effect on travel time, especially when the input flow is low. Although as the CAV penetration rate increases there are more CAVs and accordingly less HVs travelling on the road, the system travel time reduces by at most 1.5 seconds. As mentioned before, the randomness and uncertainty of HVs bring limitations to the operations of mixed traffic flow, and therefore the addition of CAV penetration serves little in performance improvement. Therefore, external controlling algorithms are needed to leverage the benefits of CAVs in the mixed traffic environment.

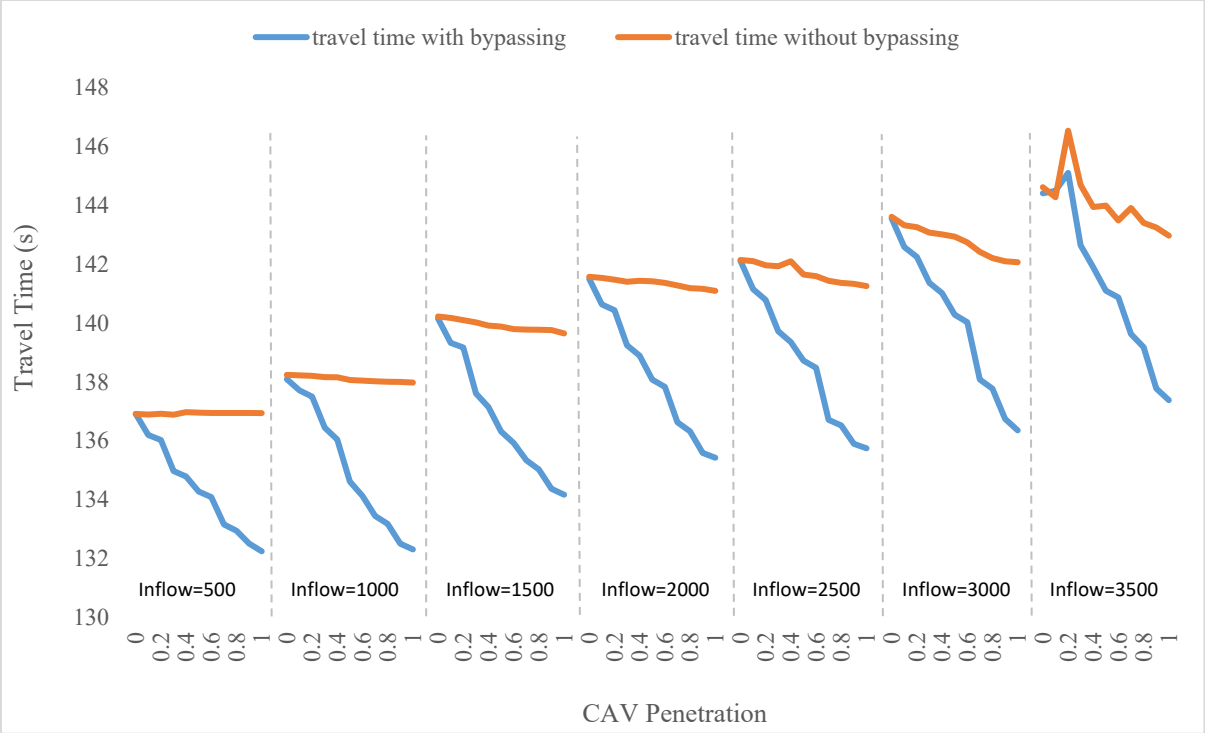

Figure 6. Travel Time Under Different Input Volumes and Different CAV Penetrations.

Under input volumes from 500 veh/h to 3500 veh/h, the proposed bypassing algorithm is proved to exhibit paramount effectiveness in reducing travel time. For example, when the CAV penetration increases from 0% to 100% under the input volume of 3000 veh/h, travel time of implementing the proposed bypassing strategy reduces from 143.6 to 136.4 seconds, while the same penetration increase without the bypassing strategy saves only 1.5 seconds. That is because, in a relatively smooth traffic flow, when a CAV platoon is blocked by a HV in front, the platoon will be prompted by the bypassing algorithm to change lanes and bypass the HV. With this bypassing algorithm, CAV platoons travel faster and more flexibly.

Despite being relatively unstable when compared to low or medium input volumes, the bypassing algorithm still has positive impacts on travel time when the input volume reaches 3500 veh/h. At a high input volume, the unstable relationship between travel time and CAV penetrations should be attributed to the congested traffic environment, where CAV platoons barely have space to change lanes.

1.6 CONCLUSION

In this study, we present an effort to propose a cooperative lane change algorithm for dealing with the complicated environment in which connected autonomous vehicles and human vehicles mix together, and furthermore, to investigate how the controlling algorithm would influence drivers' behaviors and the system operation. A microscopic simulation framework is developed in VISSIM for a two-lane freeway segment, where different car-following and lane-changing models are incorporated for CAVs and HVs. First, the VISSIM preset models, including the

Wiedemann model and a rule-based lane-changing strategy, are used to simulate human-driven vehicles. In addition, an intelligent driver model is customized to determine the CAV acceleration, and an innovative lane-changing strategy is proposed to control the interactions between CAVs and HVs. The lane-changing strategy motivates CAV platoons to move forward until approaching a preceding HV, then change lanes to bypass the HV if allowed, and move on until approaching another HV in front. The proposed lane-changing strategy is therefore called bypassing algorithm.

Through a case study with a freeway created in VISSIM, the capabilities of the developed controlling framework in forming CAV platoons, splitting platoons into sub-platoons, and changing lanes to bypass HVs, are tested in simulations. The lane changing algorithm is proved to not only benefit CAVs but also HVs in travel speed. In addition, the simulation results show the predominance of the lane changing algorithm in improving system performance for the mixed traffic flow. Specifically, under different input flows and CAV penetrations, the proposed bypassing algorithm can efficiently reduce the system travel time and improve freeway outflow performance. In comparison, the CAV technology without a bypassing algorithm has no effect in outflow performance and helps little in reducing travel time.

1.7 RECOMMENDATIONS

In theory, the bypassing algorithm can be adapted to multi-lane circumstances, one of the future works is to improve and test the algorithm for multi-lanes. In addition, we can also study the application of the proposed bypassing algorithm to traffic merging points and urban traffic intersections under a mixed environment.

CHAPTER 2. Analytical Approximation for Corridor Macroscopic Fundamental Diagram in Mixed Human and Connected Autonomous Traffic

2.1 INTRODUCTION

Intuitively, the increasing penetration of CAVs is expected to improve roadway capacities that come from the shorter reaction time of computers when compared to human drivers, but the magnitude of capacity improvement is still on debate. According to the latest literature review *(23)*, most studies concluded that introducing CAVs could improve capacity of links and intersections, especially when CAVs are at a high level of automation and penetration. In contrast, a few researchers felt uncertain about the automation and connectivity technology and questioned that low penetration of CAVs may result in a potential decrease in capacity and a decline in network performance *(24).*

Focusing on capacity analyses of CAVs in mixed traffic environment, most studies were carried out on micro-simulation platforms *(12,16,17,25)*, whereas there are very few researchers devoted to analytical approaches *(15,26,27)*. What's more, the existing analytical models developed for mixed traffic are only targeted at freeways or highways, neither of which involves intersection signals. At present, the analytical study on macroscopic characteristics of an urban road network that mixes HVs with CAVs is under-researched. Therefore, to fill this gap, this chapter provides a theoretical framework to shed light on how urban street capacity will evolve with the introduction of CAVs. First, a triangular fundamental diagram (FD) of mixed flow is developed, which takes into account reaction times of different vehicle following types, CAV penetration rate and CAV platoon size. Second, the maximum flow and backward wave speed derived from the triangular FD are used to shape the macroscopic fundamental diagram (MFD) of an urban street, given the street topology and signal timing scheme. Finally, macroscopic capacities of the urban street under different CAV penetrations are obtained from MFDs.

2.2 OBJECTIVE

- Propose an analytical MFD approach to analyze the capacity of urban street under mixed traffic environment.
- Verify the analytical method by the VISSIM simulation.

2.3 LITERATURE REVIEW

2.3.1 Capacity Analysis of Mixed Traffic

Aiming to analyze the impact of mixed CAV and HV traffic on road capacity, the existing research have provided relevant insights through the simulation platform, where microscopic features of CAVs, such as acceleration and headway time, are incorporated. Based on the new driving features of CAVs, innovative controlling algorithms, such as CAV platooning and cooperative lane-changing rules, are developed and further verified in the simulation platform. From the literature review in Table 2, a good chunk of simulation results has identified positive effects on road

capacity with the growth of CAV penetration rate, increase of platoon intensity, and reduction in headway time, but the magnitude of capacity improvement varies depending on CAV technology. For example, at the same penetration rate, different time gaps of CAVs result in quite different capacities *(25).*

Table 2. Reviewed Studies of CAV Impact on Road Capacity in Mixed Traffic

Tool	Author	Scope	Consideration	Capacity Effect
Simulation	Talebpour, and Mahmassani. *(12)*	highway	acceleration framework	**Positive:** The AV and CV technology have the potential to the throughput by more than 100%; AVs result in higher throughput compared to CVs at similar penetration rates.
	Shi, He, and Huang. *(16)*	roadway network	CAV lane-changing algorithm	**Positive:** With the CAV lane-changing algorithm, the maximum increase in capacity is 2.5%.
	Liu, et al. *(17)*	freeway	new lane-changing rules	**Positive:** CAV penetration from 0%-100%: capacity increases 90%.
	Atkins. *(24)*	link	CAV penetration; headway	**Uncertain:** Negative impact on capacity when CAV level is less than 4 (cautious behavior and long safety distance).
	Ye, and Yamamoto. *(25)*	link	CAV parameters incorporated into simulation	**Positive:** Capacity growth is largely decided by T_{ACC} (the desired net time gap of a CAV with respect to the preceding vehicle). For CAV penetration from 0%-100%: capacity increases from 2200-2500 vph ($T_{ACC} = 1.1s$); capacity increases from 2200-3300 vph ($T_{ACC} = 0.8s$); capacity increases from 2200-4500 vph ($T_{ACC} = 0.5s$).
	Amoozadeh, et al. *(28)*	highway	platoon management	**Positive:** Capacity increases with platoon size and decreases with inter-platoon spacing.
	Olia, et al. *(29)*	highway	AV/CAV car-following and lane-merging	**Positive:** AV penetration from 0%-100%: capacity remains in a range of 2046-2238 vph per lane; CAV penetration from 0%-100%: capacity increases from 2046-6450 vph per lane.
	Tilg, Yang, and Menendez. *(30)*	freeway weaving section	lane change position	**Positive:** Capacity of the studied weaving section can be increased up to 15%.
Analytical Method	Chen, et al. *(3)*	highway	AV penetration; platoon size; spacing; lane policy	**Uncertain:** Strict segregation of AVs and HVs can lead to lower capacity; mixed-use lane policies can realize higher capacities.
	Ghiasi, et al. *(14)*	highway	CAV penetration; headway; platooning intensity	**Uncertain:** Capacity is not always an increasing function of CAV platoon intensity, depending on the headways of different vehicle types.
	Levin, and Boyles. *(26)*	link	AV penetration; reaction time	**Positive:** Capacity increases with the growth of AV penetration rate and the decrement of reaction time.
	Qin, and Wang. *(27)*	link	AV penetration; reaction time	**Positive:** Capacity increases with the growth of AV penetration rate and the decrement of reaction time.

	This model	signalized corridor	CAV penetration; reaction time; platooning intensity	

Compared to extensive efforts in simulation, only a few studies attempted analytical models to characterize the capacity of mixed traffic, and some of the researchers felt uncertain about the road capacity improvement caused by the introduction of CAVs. For example, Ghiasi et al. *(15)* revealed that, contrary to the ubiquitous assumption that higher CAV penetration rates and platooning intensities always yield greater mixed traffic capacity, the two factors may not always help improve highway capacity. Furthermore, to the best of our knowledge, all of the existing analytical research on the capacity of mixed traffic flow are concentrated on highways or freeways, while the capacity of mixed urban corridors has never been studied theoretically. Therefore, the research gap will be filled in this study by establishing an analytical framework for the corridor MFD in mixed environment.

2.3.2 Analytical Approximation of MFDs

From the empirical data in Yokohama, Geroliminis and Daganzo *(31)* first verified the macroscopic fundamental diagram (MFD) as a reproducible and well-defined relationship between space-mean flow, average density and average speed on an urban network. Since then, MFD has attracted extensive attention due to its robustness at the network level. Limited factors such as network infrastructure, traffic signal control, and drivers' route choices exert difference on the shape of an MFD and its scatter *(31, 32, 33).* Nevertheless, existing studies on the factors affecting an MFD take little consideration of new technologies, like CAV. With the advent of connectivity and automation technology, vehicles can communicate with each other through vehicle-to-vehicle communications and drive themselves automatically, which will inevitably affect the operation of vehicles, and further influence the network-wide flow-density relationship (also known as MFD). To the best knowledge of the authors, until now, Mittal, Mahmassani, and Talebpour *(34)* is the only one who conducted a simulation approach to investigate dynamics of traffic flow in the presence of connected vehicles (CV) using MFD. Therefore, how the CAV technology and its application will influence the traffic flow at the network level is still an open question, the paper advances in this direction by introducing analytical MFDs to theoretically describe the macroscopic characteristics of the road network that mixes CAVs and HVs.

The estimation of MFDs of a traditional road network (full of HVs) can be categorized into three types: empirical data *(35, 36, 37),* simulation data *(38),* and analytical methods *(39, 40, 41).* The focus of this paper is on analytical estimation of MFDs, which can be further divided into three methods: method of cut (MC) *(39),* stochastic approximation (SA) *(40),* and linear program method (LP) *(41).* Recently, Tilg, Amini, and Busch *(42)* compared the three analytical estimation methods of MFDs to empirical data, and found that the MC and LP resemble each other and have much higher accuracies than the SA in approximating an arterial MFD. Therefore, the MC is adopted in this chapter to derive the corridor MFDs. Leveraging the concept of MFD, this study

is the first to analytically investigate macroscopic characteristics of an urban arterial in the presence of CAVs.

2.4 METHODOLOGY

2.4.1 Fundamental Diagram of Mixed Traffic Stream

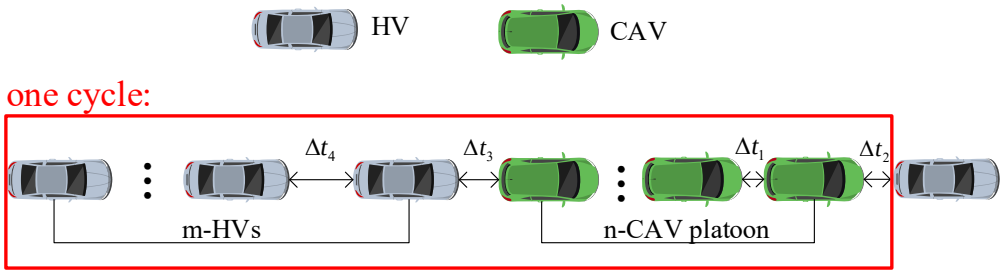

Figure 7. One Traffic Stream Consisting of m-HVs and One n-CAV Platoon.

In this section, we first formulate the density-speed relationship for a single-lane link. For simplification, the mixed traffic flow in a link is divided into periodically distributed traffic streams, each of them is consisted of n CAVs as one platoon followed by m HVs, as shown in Figure 7. The same as Chen et al. *(3),* we assume that both CAVs and HVs travel at a constant free-flow speed of u_f until they reach their respective critical spacings (corresponding to maximum link flow), below which they enter the car-following mode. During the car-following process, different reaction times are expected for different vehicle following types, and in general, CAVs have smaller reaction times than those of HVs. In this chapter, we differentiate four different reaction times based on following pairs: Δt_1 for a CAV following a CAV within a CAV platoon, Δt_2 for a CAV platoon leader following a HV, Δt_3 for a HV following a CAV, and Δt_4 for a HV following a HV. Take the traffic stream in Figure 7 as the proxy for the whole traffic flow dynamics. Density k (veh/m) of the traffic stream is defined as the average number of vehicles per unit length, and the critical density of the mixed traffic stream k_{cri}^{mix}, at which all the vehicles travel in the car-following mode at free-flow speed u_f, is calculated in Equation (3).

$$k_{cri}^{mix} = \frac{1}{u_f \cdot \left[\Delta t_4 \cdot (1-p) + \Delta t_1 \cdot p + \frac{p}{n} \cdot (\Delta t_2 + \Delta t_3 - \Delta t_1 - \Delta t_4)\right] + d_j} \quad \text{Eq. (3)}$$

Where $p = \frac{n}{m+n}$ denotes the CAV penetration rate in the mixed traffic stream, d_j is the jam distance (including the vehicle length), and we assume each vehicle has the same jam distance. It can be inferred from formula (3) that the critical density of a mixed traffic stream is bearing upon CAV penetration rate p, reaction times of different vehicle following types $(\Delta t_1, \Delta t_2, \Delta t_3, \Delta t_4)$, and CAV platoon size n (we call it CAV platoon intensity).

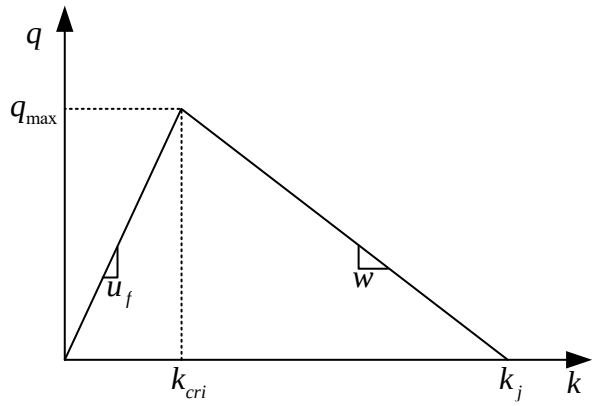

Figure 8. Fundamental Diagram.

As shown in Figure 8, the triangular fundamental diagram (FD) *(43)* is commonly used to represent the flow-density relationship in equilibrium traffic. The functional form of the flow-density ($q - k$) relation is expressed as Equation (4).

$$q = \begin{cases} u_f \cdot k & if\ k \le k_{cri} \\ w \cdot (k_j - k) & otherwise \end{cases} \quad \text{Eq. (4)}$$

Where u_f is the free-flow speed, w denotes the backward wave speed, k_j means the jam density, and k_{cri} represents the critical density that maximizes traffic flow, q_{max} denotes the maximum flow. Relating Equation (3) to Equation (4), the maximum flow of the mixed traffic stream q_{max}^{mix} is expressed as formula (5).

$$q_{max}^{mix} = \frac{u_f}{u_f \cdot \left[\Delta t_4 \cdot (1-p) + \Delta t_1 \cdot p + \frac{p}{n}(\Delta t_2 + \Delta t_3 - \Delta t_1 - \Delta t_4)\right] + d_j} \quad \text{Eq. (5)}$$

The backward wave speed of the mixed traffic stream w^{mix} is formulated as Equation (6).

$$w^{mix} = -\frac{q_{max}^{mix}}{k_{cri}^{mix} - k_j} = -\frac{d_j}{\Delta t_1 \cdot p + \Delta t_4 \cdot (1-p) + \frac{p}{n}(\Delta t_2 + \Delta t_3 - \Delta t_1 - \Delta t_4)} \quad \text{Eq. (6)}$$

Clearly, not only the critical density k_{cri}^{mix}, but also the backward wave speed w^{mix} and the maximum flow q_{max}^{mix} of the mixed traffic stream depend on CAV penetration rate p, reaction times of different vehicle following types ($\Delta t_1, \Delta t_2, \Delta t_3, \Delta t_4$), and the CAV platoon intensity n.

2.4.2 Monte Carlo Method for the CAV Platoon Intensity

As in chapter 2, a 2-kilometer freeway is simulated in VISSIM, where different inflows from 500 to 3500 veh/h and CAVs from 0% to 100% penetration rates are gradually loaded. Consecutive CAVs in each lane are treated as a CAV platoon and the number of consecutive CAVs is called the platoon size. CAV platoon intensity refers to the average size of a CAV platoon. The simulation result is shown in Figure 9, for each scenario of inflow, CAV platoon intensity increases

exponentially with the CAV penetration rate. However, without limiting the maximal size of a CAV platoon, the CAV penetration of 1.0 (100%) resulted in a very large CAV platoon intensity, which was inconsistent with the limitation of the vehicle-to-vehicle communication range. Therefore, as suggested in *(44)*, the maximal platoon intensity in this chapter is pre-determined as 20, below which the CAV platoon intensity is dependent on the CAV penetration rate. In addition, the CAV platoon intensity seems in connection with traffic inflows. Nevertheless, it can be explored from the green box of Figure 9 that, except for the case of low inflow and CAV penetration of 1.0, the increasing trends of CAV platoon intensity with the CAV penetration rate are similar for different inflows. Thus, for simplification, this report mainly studies traffic inflows of medium or above. In this case, only CAV penetration rate is accounted as a factor for CAV platoon intensity.

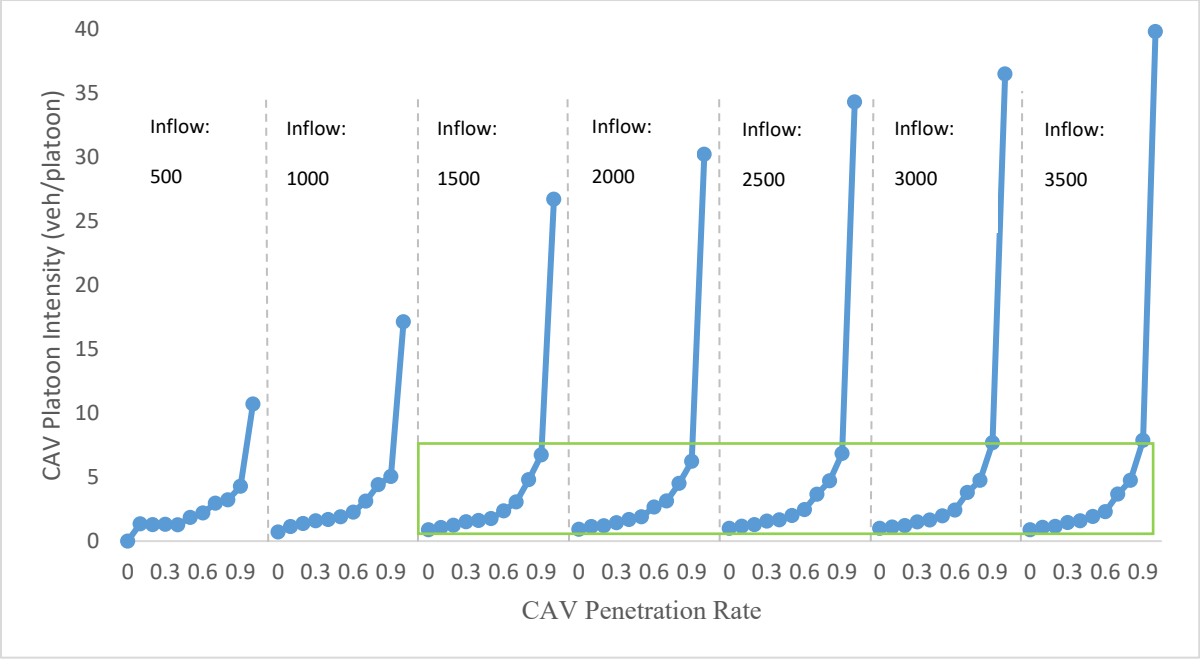

Figure 9. Simulated Platoon Intensity under Different Inflows, Different CAV Penetration Rates and Different Lane-changing Strategies.

To study the general relationship between the CAV platoon intensity n and CAV penetration rate p, Monte Carlo method is exploited in this chapter. In the Monte Carlo simulation, an infinite number of vehicles, including CAVs with penetration rate of p and HVs with penetration of $(1-p)$, are randomly distributed on a single-lane link. Under the medium or above traffic flow, adjacent CAVs are assumed to form a platoon until the maximal size of a CAV platoon (set as 20 in this report) is achieved, and the CAV platoon intensity is defined as the average size of a CAV platoon. The Monte Carlo simulation result is shown in Figure 10.

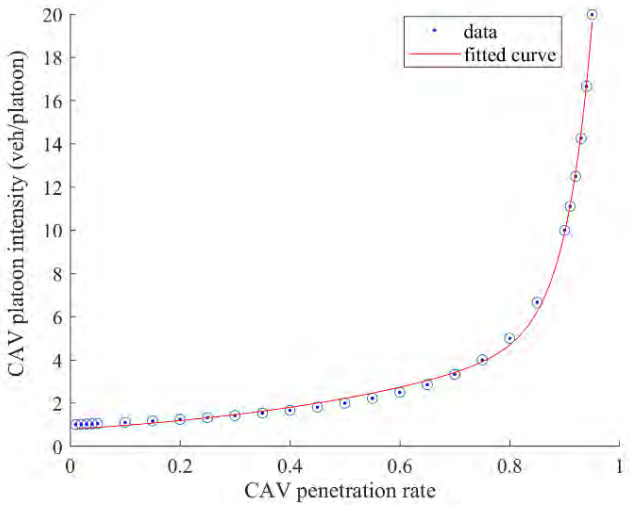

Figure 10. Monte Carlo Simulation Result and the Fitting Curve.

In Figure 10, the data points (CAV penetration rate, CAV platoon intensity) fit the two-term exponential model perfectly, as seen in Equation (7). The sum of squared residuals (SSE) of the exponential fitting model is 1.0497, indicating that the fitting model has a small random error component. R-square value is 0.9987, meaning that the exponential fit explains 99.87% of the total variation in the data about the average.

$$n = \begin{cases} 0 & p = 0 \\ 0.7917e^{2.063p} + 2.234 \times 10^{-8}e^{21.32p} & 0 < p < 0.96 \\ 20 & 0.96 \le p \le 1 \end{cases} \quad \text{Eq. (7)}$$

Interpolating CAV platoon intensity in Equation (7) into Equations (5) and (6), the maximum flow and backward wave speed of the mixed traffic stream can be formulated as formula (8) and (9), on which basis a mixed FD is shaped.

$$q_{max}^{mix} = \begin{cases} \dfrac{u_f}{u_f \cdot \left[\Delta t_4 \cdot (1-p) + \Delta t_1 \cdot p + \dfrac{p \cdot (\Delta t_2 + \Delta t_3 - \Delta t_1 - \Delta t_4)}{0.7917 \cdot e^{2.063p} + 2.234 \times 10^{-8} \cdot e^{21.32p}}\right] + d_j} & 0 \le p < 0.96 \\ \dfrac{u_f}{u_f \cdot \left[\Delta t_4 \cdot (1-p) + \Delta t_1 \cdot p + \dfrac{p \cdot (\Delta t_2 + \Delta t_3 - \Delta t_1 - \Delta t_4)}{20}\right] + d_j} & 0.96 \le p \le 1 \end{cases} \quad \text{Eq. (8)}$$

$$w^{mix} = \begin{cases} -\dfrac{d_j}{\Delta t_1 \cdot p + \Delta t_4 \cdot (1-p) + \dfrac{p \cdot (\Delta t_2 + \Delta t_3 - \Delta t_1 - \Delta t_4)}{0.7917 \cdot e^{2.063p} + 2.234 \times 10^{-8} \cdot e^{21.32p}}} & 0 \le p < 0.96 \\ -\dfrac{d_j}{\Delta t_1 \cdot p + \Delta t_4 \cdot (1-p) + \dfrac{p}{20} \cdot (\Delta t_2 + \Delta t_3 - \Delta t_1 - \Delta t_4)} & 0.96 \le p \le 1 \end{cases} \quad \text{Eq. (9)}$$

It is noteworthy that when $0 < p < 0.96$, the formula in the red box of Equation (8) is a non-monotonically function that increases first and then decreases with p. Therefore, the maximum flow on the mixed FD q_{max}^{mix} (also called link capacity) is not always an increasing function of CAV penetration rate but depends on reaction times of different vehicle following types. It is self-

evident that the reaction time between two CAVs (Δt_1) should be smaller than that between two HVs (Δt_4), based on which, if $\Delta t_2 + \Delta t_3 \leq \Delta t_1 + \Delta t_4$, the link capacity will increases with the CAV penetration rate. However, it seems counterintuitive that when $\Delta t_2 + \Delta t_3 > \Delta t_1 + \Delta t_4$, the link capacity first decreases and then increases with the CAV penetration rate. Such conclusion reminds traffic planners and managers to treat CAV technologies carefully in the mixed traffic environment. If the reaction times of different vehicle types are not properly handled, the introduction of CAVs may have a negative effect on traffic flow capacity. How the urban corridor capacity changes with the CAV penetration will be demonstrated in chapter 2.5.

2.4.3 Macroscopic Fundamental Diagram of Mixed Traffic on Homogeneous Streets

Consider a homogeneous corridor consisting of a series of successive links of uniform length l, each one delimited by the same traffic signal settings of green time G, cycle time C and offset δ. Analytic method developed for obtaining macroscopic fundamental diagrams (MFDs) of urban corridors has the origin from Daganzo and Geroliminis *(39)*, where traffic dynamics is represented by the Lighthill, M.J and Whitham, G.B. (LW) model *(45)* and a triangular fundamental diagram (FD) with free flow speed u_f, backward wave speed w and maximum flow q_{max}. An MFD is capped by a set of cuts in the analytic method of Daganzo and Geroliminis, which we call method of cut (MC). The principle of MC is demonstrated in Figure 11, where a forward-moving observer traverses two consecutive intersections ($\gamma = 1,2$) at speed u_f, until it is stopped by a red signal, resulting in the delay of $d_{forward}$. Likewise, a backward-moving observer travels at speed w, stops in a red phase, leading to the delay of $d_{backward}$, and the reversal of moving direction changes offset to δ_w. The three families of upper cuts (Q_1, Q_2, Q_3) in Figure 11(b) correspond to the observers in Figure 11(a) that move at speeds (u_f, 0, and $-w$).

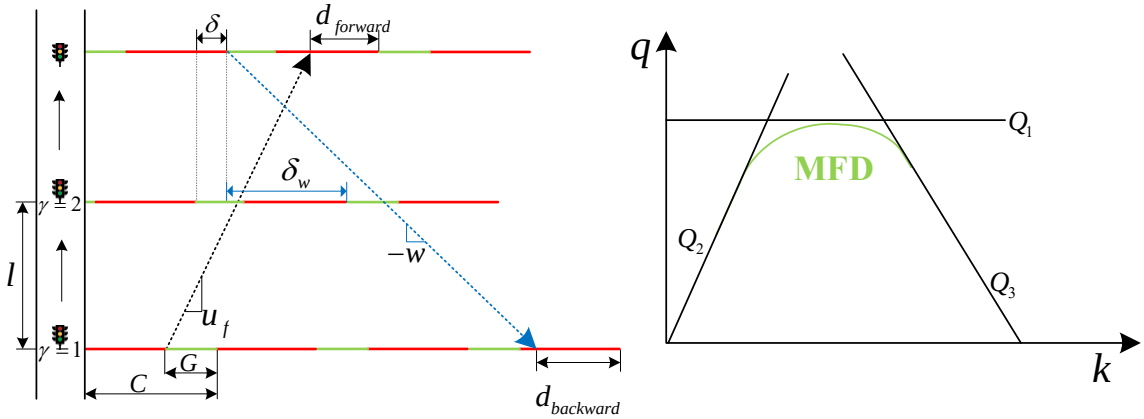

(a) (b)

Figure 11. Analytical Macroscopic Fundamental Diagram from Method of Cut; (a) Time-space movements of observers (b) Three upper cuts for an MFD.

The method of cut (MC), based on triangular FD, was developed for MFD in traditional urban corridors, where all the vehicles are driven by humans. However, the penetration of CAVs have brought changes to the triangular FD, especially in the backward wave speed w^{mix} and maximum

flow q_{max}^{mix}. Therefore, utilizing the principle of MC, the mixed FD derived from the previous section can be used to form the MFD of urban corridors in mixed traffic flow. The same as Daganzo and Geroliminis *(39)*, three families of upper envelopes that jointly bound the MFD from above are drawn in this chapter based on observers' speeds.

$$Q_1 = q_{max}^{mix} \cdot \frac{G}{C} \quad \text{Eq. (10)}$$

Where Q_1 is the first family of cut that uses a stationary observer at each signal intersection, q_{max}^{mix} is the maximum flow in the mixed FD, G and C are the green and cycle time at each intersection respectively.

$$d_{forward} = C \cdot \left(\left\lceil \frac{\gamma_{max}(\frac{l}{u_f} - \delta)}{C} \right\rceil - \frac{\gamma_{max}(\frac{l}{u_f} - \delta)}{C} \right) \quad \text{Eq. (11)}$$

$$u_{forward} = \frac{\gamma_{max} \cdot l}{d_{forward} + \gamma_{max} \cdot \frac{l}{u_f}} \quad \text{Eq. (12)}$$

$$f_{forward} = \frac{d_{forward} - C + G}{d_{forward} + \gamma_{max} \cdot \frac{l}{u_f}} \quad \text{Eq. (13)}$$

$$Q_2 = k \cdot u_{forward} + q_{max}^{mix} \cdot f_{forward} \quad \text{Eq. (14)}$$

Where Q_2 is the second family of cut that uses an observer moving forward along the corridor at speed u_f, γ_{max} denotes the number of links a fast observer traverses between consecutive intersections without stopping ($\gamma_{max} = 2$ in Figure 11(a)), l is the link length between consecutive intersections, δ is the offset of each traffic signal, $d_{forward}$ represents the delay at each stop of a forward-moving observer, $u_{forward}$ is the average speed of the forward-moving observer, and $f_{forward}$ is the fraction of time that the forward-moving observer spends artificially stopped in green phases due to extended red phases.

$$\delta_w = C - \delta \quad \text{Eq. (15)}$$

$$d_{backward} = C \cdot \left(\left\lceil \frac{\gamma_{max} \cdot \left(\frac{l}{w^{mix}} - \delta_w\right)}{C} \right\rceil - \frac{\gamma_{max} \cdot \left(\frac{l}{w^{mix}} - \delta_w\right)}{C} \right) \quad \text{Eq. (16)}$$

$$u_{backward} = \frac{\gamma_{max} \cdot l}{d_{forward} + \gamma_{max} \cdot \frac{l}{w^{mix}}} \quad \text{Eq. (17)}$$

$$f_{backward} = \frac{d_{forward} - C + G}{d_{forward} + \gamma_{max} \cdot \frac{l}{w^{mix}}} \quad \text{Eq. (18)}$$

$$r = \frac{(u_f + w^{mix}) \cdot q_{max}^{mix}}{u_f}$$ Eq. (19)

$$Q_3 = -k \cdot u_{backward} + q_{max}^{mix} \cdot f_{backward} + r \cdot \frac{u_{backward}}{w^{mix}}$$ Eq. (20)

Where Q_3 is the third family of cut that uses an observer travelling backward along the corridor at speed w^{mix}, δ_w is the signal offset from the backward direction, r is the maximum rate of the backward-moving observer being passed, $d_{backward}$, $u_{backward}$ and $f_{backward}$ are the delay, average speed, and fraction of time spent in extended red phases of the backward-moving observer.

2.5 RESULTS

2.5.1 Scenario Setting

As in reference *(39)*, we study the urban corridor of San Francisco, with roughly the same scenario settings. The parameters used in estimating MFDs include the average link length $l = 122.9m$, free-flow speed $u_f = 13.4m/s$, jam distance $d_j = 7.7m$, green time of each signal $G = 21s$, cycle time of each signal $C = 60s$, offset of each signal $\delta = 3s$, and $\gamma_{max} = 2$. Turning movements are not considered in our experiments.

2.5.2 Corridor Capacity for $\Delta t_2 + \Delta t_3 \leq \Delta t_1 + \Delta t_4$

We first set the reaction time of a CAV following a CAV as 0.5s ($\Delta t_1 = 0.5s$), a CAV following an HV as 0.9s ($\Delta t_2 = 0.9s$), an HV following a CAV as 1.0s ($\Delta t_3 = 1.0s$), and an HV following an HV as 1.5s ($\Delta t_4 = 1.5s$), so that $\Delta t_2 + \Delta t_3 \leq \Delta t_1 + \Delta t_4$. To investigate the impact of CAV penetration rate on the mixed corridor MFD and capacity comprehensively, the proposed analytical method is applied to full spectra of CAV penetration rates ranging from 0.0 to 1.0 with interval of 0.1, the result is depicted in Figure 12.

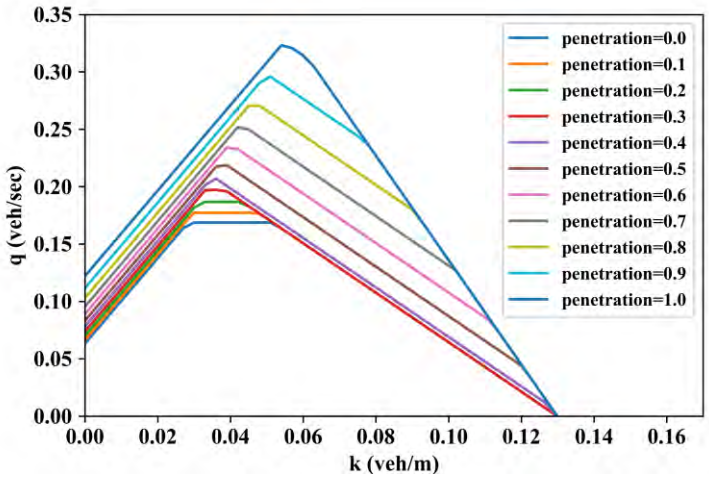

Figure 12. Analytical MFD Evolution with CAV Penetration When $\Delta t_2 + \Delta t_3 \leq \Delta t_1 + \Delta t_4$.

It can be seen from Figure 12 that the corridor capacity increases with the CAV penetration rate, and the magnitude of capacity growth accelerates with the increase of CAV penetration. This phenomenon may benefit from the reaction times ($\Delta t_1 = 0.5s$, $\Delta t_2 = 0.9s$, $\Delta t_3 = 1.0s$ and $\Delta t_4 = 1.5s$) that $\Delta t_2 + \Delta t_3 \leq \Delta t_1 + \Delta t_4$ can result in a monotonic growth of link capacity with CAV penetration rates. In addition, the critical density that makes the corridor flow reach capacity also presents a monotone increasing trend with the growing CAV penetration rates.

2.5.3 Corridor Capacity for $\Delta t_2 + \Delta t_3 > \Delta t_1 + \Delta t_4$

As alluded to previously, $\Delta t_2 + \Delta t_3 > \Delta t_1 + \Delta t_4$ will lead to a drop of link capacity first and then a slow recovery, but how the reaction time will influence the corridor capacity is yet to be investigated. Here we set the reaction times of a CAV following a CAV as 0.5s ($\Delta t_1 = 0.5s$), a CAV following an HV as 2.0s ($\Delta t_2 = 2.0s$), an HV following a CAV as 1.0s ($\Delta t_3 = 1.0s$), and an HV following an HV as 1.0s ($\Delta t_4 = 1.0s$), so that $\Delta t_2 + \Delta t_3 > \Delta t_1 + \Delta t_4$. Figure 13 shows the MFD evolution with CAV penetration rates from 0.0 to 1.0. Note that, the corridor capacity decreases when the CAV penetration increases from 0.0 to 0.2, then gradually recovers until the original level of corridor capacity is restored at CAV penetration rate of 0.6, thereafter, the corridor capacity increases with the growth of CAV penetration rate. In other words, under reaction time settings in this experiment, the CAV technology exerts advantages in corridor capacity only when CAV penetration rate is equal to or larger than 0.6, and low penetration of CAVs even results in a decline in corridor capacity.

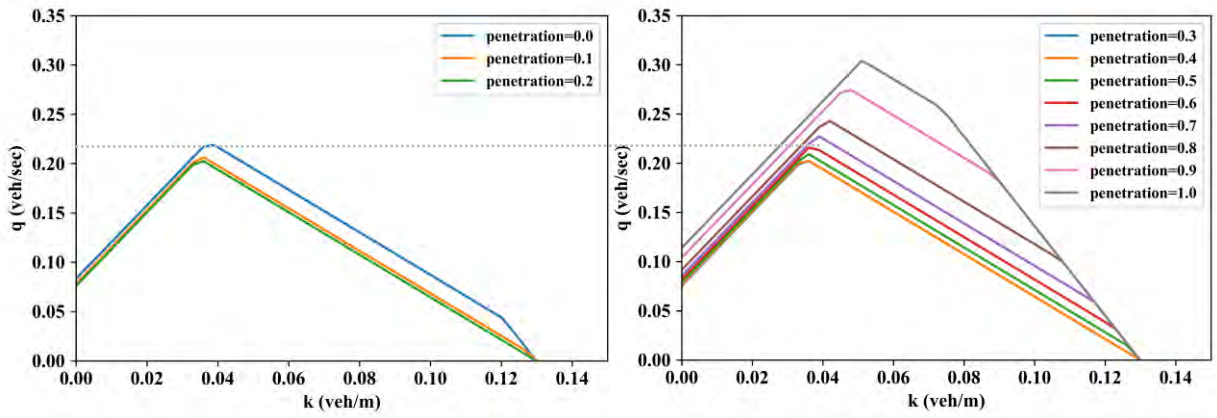

(a) (b)

Figure 13. Analytical MFD Evolution with CAV Penetration When $\Delta t_2 + \Delta t_3 > \Delta t_1 + \Delta t_4$; (a) CAV penetration rate from 0.0 to 0.2 (b) CAV penetration rate from 0.3 to 1.0.

By comparing Figure 13 with Figure 12, it suggests that $\Delta t_2 + \Delta t_3 \leq \Delta t_1 + \Delta t_4$ brings greater improvement in the corridor capacity than $\Delta t_2 + \Delta t_3 > \Delta t_1 + \Delta t_4$ for the whole spectra of CAV penetration rates. The analytical results also verify that higher CAV penetration rates may not always yield greater mixed traffic capacity of urban corridors. Therefore, before CAV technology is put into practice, traffic operators should be aware of the sensitivity of road capacity to reaction time of different vehicle types.

2.5.4 Comparison with Simulation

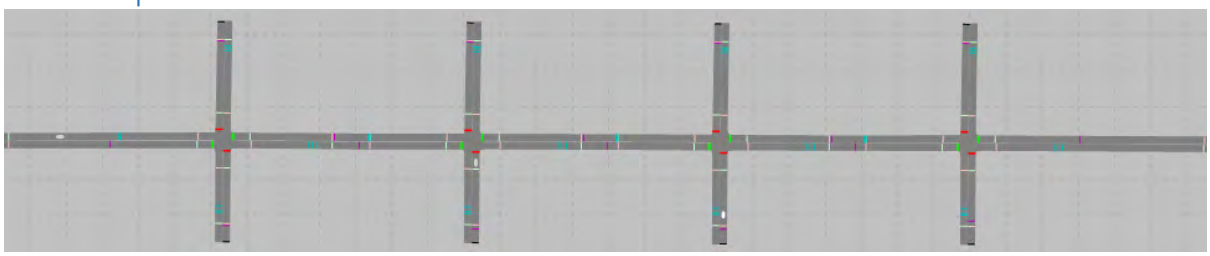

Figure 14. Corridor Simulation in VISSIM.

In this section we compare the proposed analytical approximation of corridor MFD with traffic simulation data obtained by PTV VISSIM. As shown in Figure 14, the urban corridor, consisting of four signal intersections, is simulated in VISSIM 11, and the scenario setting is the same as that in the analytical experiment (length of each link $l = 122.9m$, the free-flow speed $u_f = 13.4m/s$, the jam distance $d_j = 7.7m$, the green time of each signal $G = 21s$, the cycle time of each signal $C = 60s$, and the offset of each signal $\delta = 3s$). In order to satisfy the jam distance of 7.7 meters, the standstill distance of vehicles is set as 3.2 meters except vehicle length of 4.5 meters. In addition, two vehicle types named "CAV" and "HV" are created, whose driving behavior are simulated by the default car following model in VISSIM, and parameters are customized according to the change in reaction times that CAVs would bring. In this experiment, the headway time of a CAV following a CAV is set as 0.5s, that of a CAV following a HV is 2.0s, that of an HV following an HV is 1.0s, and that of an HV following a CAV is 1.0s. Besides, the longitudinal oscillation of a CAV following a CAV is set as 0, indicating more stable following behaviors between consecutive CAVs. The other parameters not mentioned here remain the default values in VISSIM.

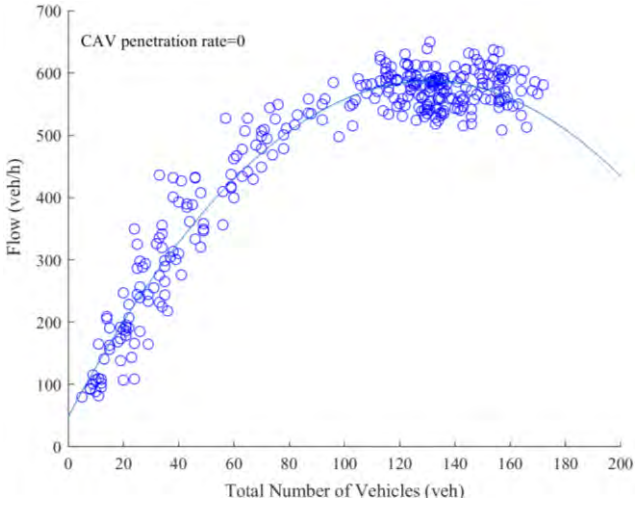

(a)

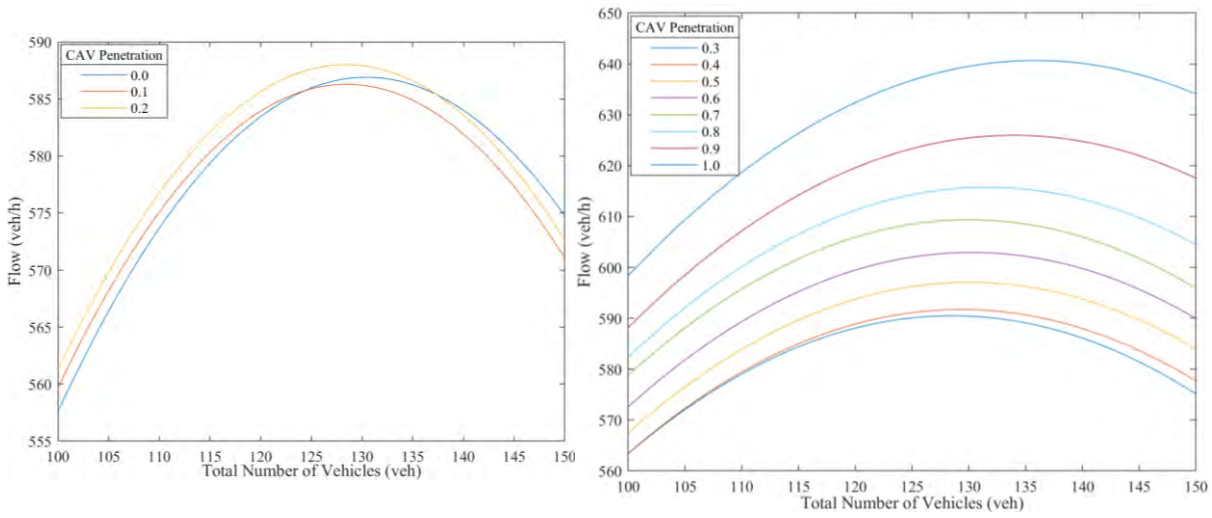

(b) (c)

Figure 15. Simulated MFD Evolution with CAV Penetration When $\Delta t_2 + \Delta t_3 > \Delta t_1 + \Delta t_4$; (a) MFD fitting curve of simulated data points; (b) Fitted MFDs evolve with CAV penetration rates from 0.0 to 0.2; (c) Fitted MFDs evolve with CAV penetration rates from 0.3 to 1.0.

To test the influence of CAV penetration rate in the corridor capacity, a Python script is used to communicate with VISSIM through COM interface, traversing the CAV penetration rate from 0.0 to 1.0 with an interval of 0.1. During each simulation, the total number of vehicles and traffic flow are aggregated, as shown in Figure 15(a), and then fitted to a quadratic parabolic curve which is regarded as an MFD *(46, 47)*. The corridor capacity can be reflected by the cusp of MFD. With the setting of $\Delta t_2 + \Delta t_3 > \Delta t_1 + \Delta t_4$ ($\Delta t_1 = 0.5s$, $\Delta t_2 = 2.0s$, $\Delta t_3 = 1.0s$, $\Delta t_4 = 1.0s$), the MFD evolution with CAV penetration rate is presented in Figure 15(b) and Figure 15(c). The corridor capacity experiences a slight drop when CAV penetration rate increases from 0.0 to 0.1, then a slow increase of capacity is observed when CAV penetration rate ranges from 0.2 to 0.5. After 50% penetration of CAVs, the improvement of corridor capacity becomes more prominent with the growth of CAV penetration. Such phenomenon is similar to the conclusion obtained from analytical method in the previous section.

2.6 CONCLUSION

This chapter is the first study that developed an analytical methodology to study how the macroscopic capacity of an urban corridor will evolve with the advent of CAVs. Initially, the link capacity and backward wave speed of a mixed traffic stream was formulated and described as a mixed FD, taking the reaction time of different vehicle types, CAV penetration rate, and CAV platoon intensity into account. Particularly, through the Monte Carlo simulation, the CAV platoon intensity was expressed as an exponential function of CAV penetration rate. Based on the mixed FD, the upper bound of an MFD for a mixed urban corridor is derived theoretically through the method of cuts (MC). Then, two numerical experiments were carried out to implement the proposed methodology. The first experimental results revealed a monotonic increasing

relationship between corridor capacity and CAV penetration rate for $\Delta t_2 + \Delta t_3 \leq \Delta t_1 + \Delta t_4$. However, when $\Delta t_2 + \Delta t_3 > \Delta t_1 + \Delta t_4$ in the second experiment, the corridor capacity suffered slight reduction for low CAV penetrations. The experimental results remind traffic operators and vehicle industries to be careful of potential impacts of different CAV technologies on corridor capacity, especially pay attention to the reaction time settings of different vehicle types for low CAV penetration rates. Finally, simulation tests were conducted in VISSIM 11 to validate the usefulness of the proposed analytical method on mixed corridors, and the simulation results showed similarity with the results of analytical numerical experiments.

2.7 RECOMMENDATIONS

This study can be extended in a number of directions in the future. First, this study adopted MC to draw the upper bounds of MFDs, how the other analytical methods for MFDs (e.g. SA, LP) would perform in mixed corridors is full of interest. Second, this paper is focused on analytical MFDs in urban corridors, which can be further extended to urban networks.

CHAPTER 3. Macroscopic Fundamental Diagram Based Discrete Transportation Network Design

3.1 INTRODUCTION

CAVs could encourage longer distance travel and increase total vehicle kilometre travelled (VKT) by reducing travel and parking costs and by providing improved mobility to those who are too young to drive, old people, and the disabled. Therefore, the advent of CAVs will bring changes to the induced travel demand associated with CAVs. Truong et al. (2017) explored the influence of autonomous vehicles (AVs) on vehicle trip and found that, AVs would lead to an overall increase of 4.14% in daily trips in Victoria, Australia. The 76+ age group would have the largest increase of 18.5%, followed by the 18–24 age group and the 12–17 age group with 14.6% and 11.1% respectively *(1)*.

With the substantial increase in travel demand and existing limited road space, high priorities of governments and the general public have been given to the problem of traffic congestion. Standing at the perspective of supply side, great efforts have been undertaken to mitigate traffic congestion, among which infrastructure construction such as expanding road capacity or building a new road is a common approach. These efforts could be associated with transportation network design problem (NDP) which is recognized as a strategical decision-making problem with the objective to improve the system efficiency. Depending on the continuity of involved decision variables, the NDP can be categorized into 1) the continuous network design problem (CNDP) aiming to optimize road network performance by the expansion of road capacity, 2) the discrete network design problem (DNDP) proposed to optimize road network performance by adding new road sections to an existing network, and 3) the mixed network design problem (MNDP) simultaneously taking CNDP and DNDP into consideration *(48)*. This research selects DNDP as the topic.

Traditionally, most of the DNDPs focus on minimizing the total travel cost within a given budget while being subject to user equilibrium constraints. However, the network travel cost is hyper-sensitive to the input information, small perturbations to the origin-destination (OD) tables or small changes to drivers' route choices can drastically change the traffic congestion indexes such as the total travel time, the number of bottlenecks, delay, density and other network outputs *(49)*. That means, although the newly built road can abate the network travel time most at present, when the OD demand varies in the future, the constructing strategy may not meet the original design expectations anymore, or even result in a higher cost than the original network.

With these observations, in this study we attempted a new approach to the measurement of network-wide performance in light of the MFD concept. An MFD demonstrates a robust demand-insensitive relationship between network vehicle density and space-mean flow, which can also be expressed as the relationship between vehicle accumulations and network outflow *(49)*. MFD is an attribute of the network infrastructure and the control strategy implemented. It implies that fluctuations of traffic demand would not change the shape of MFD, but modifying the road

infrastructure or signal control can make a difference to an MFD. In order to circumvent the demand uncertainty problems of a traditional traffic flow model, the MFD-based network characterization method is employed as the performance evaluation index of a network in this chapter.

For a DNDP, the chapter devotes to applying the MFD method to the improvement of network capacity so as to mitigate traffic congestion by optimizing the topology of an urban road network. A bi-level programming model is propounded where the upper level seeks the goal of maximizing network capacity subject to limited budgets, and the lower level presents a user equilibrium model to reflect traffic state under different road construction plans.

3.2 OBJECTIVE

- Implement MFD in network design problem.

3.3 LITERATURE REVIEW

LeBlanc (1975) first addressed the discrete network design problem (DNDP) for determining which links should be added to an urban road network to ease traffic congestion *(50)*. To explicitly describe the network design problem, LeBlanc developed a bi-level programming model, which has an upper level minimizing the total travel time and a lower level reflecting user equilibrium routes of vehicles for a given road network configuration. Then extensive research has been carried out to deal with the network design problem, but a large majority of the earlier studies only concentrated on the objective of minimizing the system travel time to improve the network performance. As the research moves along, the researchers gradually shift their attention to equity, sustainability, consumer surplus, reserve capacity and accessibility, etc. For example, Behbahania et al. (2019) incorporated social equity into transportation network planning for simultaneously minimizing total travel time and achieving social equity objectives *(51)*. Jiang and Szeto (2015) formulated a multi-objective network design model maximizing both the increase in consumer surplus and the reduction in the health cost to measure the network performance and health condition of residents respectively. In the health cost function, three sustainability indicators including traffic emissions, noise, and accidents were considered *(52)*. After comparing the objectives of minimizing the total system cost and maximizing the network reserve capacity, Yang and Wang (2002) found that the equivalence relationship of the two objectives varies by level of congestion. That means, the higher the congestion level is, the objective of maximizing the reserve capacity deviates farther from the objective of minimizing the total travel cost. Thus, the authors suggested a combined target by applying different weightings on the two objectives *(53)*. Recognizing the difference between reserve capacity and system travel time, Miandoabchi et al. (2013) proposed a three-objective model that involves one reserve capacity and two new travel related objective functions *(54)*. Di et al. (2018) combined traffic flow and accessibility together to straightforwardly measure whether travellers could reach their destinations *(48)*. To summarize the above research studies, when considering other aspects like equity, sustainability, consumer surplus, reserve capacity and/or accessibility, most studies proposed multi-objective models still including travel time as one of the objectives to optimize the network performance.

However, travel time as a performance indicator is susceptible to network input, such as travel demand, which will face uncertainty in the future. Therefore, it is necessary to establish a stable and robust measurement index for evaluating road network performance.

In this study, we adopted MFD to circumvent the demand uncertainty problem of traditional models for evaluating the network improvement. Geroliminis and Daganzo (2008) first verified the existence of MFD linking space-mean flow, density and speed on a large urban area through the field experiment data of Yokohama *(31)*. As shown in Figure 16, the shape of an MFD illustrates a unimodal relationship between weighted average flow and density. There is a similar relationship between outflow and accumulation as well, because the ratio of network flow and outflow is constant *(31)*. Generally, there are three parts in an MFD, representing unsaturated, saturated and oversaturated traffic states respectively. In the case of unsaturated state, network flow increases with the network density. When more and more vehicles come into the network, the network space-mean density keeps growing and the consequential network flow gradually grows to its capacity, which is known as the saturated state. When more vehicles are added into the road network at the maximum flow, the network flow will start to decrease until a gridlock, also considered as an oversaturated state, occurring if the network density continues increasing.

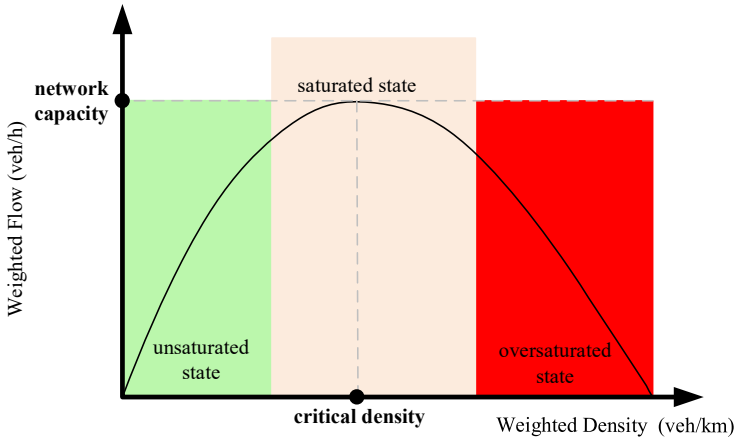

Figure 16. General Shape of an MFD.

One of the most intriguing observations of Geroliminis and Daganzo (2008) showed that MFD is a property of the road network itself and is independent of demand. More specifically, the maximum flow (or outflow) of a road network remains invariant when the demand changes, but on the other hand, variations in road spatial distribution can result in different MFDs of the same neighbourhood *(31)*. Likewise, the space-mean flow is maximum for the same value of critical vehicle density, irrespective of the time-dependent OD tables *(55)*. These steady and elegant properties of MFDs can be fully utilized to develop a robust network design strategy for meeting stochastic demand in the future.

Until now, to our knowledge, there is little research undertaken for the network design problem with an application of the MFD measure. In this regard, our study attempts to fill in the gap for

further development of NDP. From the modelling standpoint, this study takes network capacity (maximum network flow) in an MFD as the measurement of network performance and formulates a bi-level model where the upper level determines which new links from the candidates should be built in order to achieve the highest network capacity, while the lower level generates a new user equilibrium every time when the decision variable in the upper level changes.

3.4 METHODOLOGY

We use a bi-level programming to describe the underlying process of DNDP, where the transport planner determines the detailed network design strategy in the upper level, and over the newly extended network based on each construction strategy, travellers choose their routes in a user optimal manner in the lower level. The objective of this model is to maximize the network capacity by selecting the optimal network design scheme. The following notations in Table 3 are used in the model formulation.

Table 3. Notations and Definitions in Model Formulation

Notation	Detailed Definition
A	Set of all links in a new network
A^0	Set of all links in the original road network
$\bar{A}$	Set of candidate links to be built
B	Total budget for building new links
C_a^k	Capacity of link a under demand scenario k
D	Set of OD pairs
K	Set of random OD demand scenarios
P_{rs}^k	Set of routes between OD pairs rs under demand scenario k
Q	Optimal network capacity
Q_k	Network weighted flow under demand scenario k
Z^k	Total travel time of equilibrium flow under demand scenario k
a	Link index
b_a	Construction cost of link a, $a \in \bar{A}$
$f_{p,k}^{rs}$	Flow on route $p \in P_{rs}$ between OD pairs rs under traffic demand scenario k
k	Index of a random OD demand scenario
l_a	The length of link a
q_k^{rs}	Travel demand between OD pairs rs under demand scenario k
$t_a^{k,f}$	Free-flow travel time on link a under demand scenario k
$t_a^k(x_a^k)$	Travel time on link a relating to flow x_a^k under demand scenario k
x_a^k	Traffic flow on link $a \in A$ under demand scenario k
y_a	Binary decision variable which equals 1 if and only if link $a \in \bar{A}$ is to be built, and 0 otherwise
$\delta_{a,p}^{rs,k}$	A binary variable which equals 1 if the route p between OD pairs rs under traffic demand scenario k passes link a, and 0 otherwise

3.4.1 Upper-level Network Design

Given an existing road network A^0, if the transportation infrastructures gradually have difficulty in undertaking the current travel demand, transport planners can build one or more new roads from candidates $\bar{A}$ within limited budget B to increase traffic supply and alleviate traffic

congestion. The set K contains randomly generated traffic demand scenarios, where the generation and attraction of each traffic zone are diversified.

To evaluate the effectiveness of each feasible construction strategy for varied traffic demands, MFD-based network capacity is proposed in this model for measuring the network performance. The network capacity is defined as the maximum network flow which is linearly related to network outflow. Therefore, the network capacity can describe how many vehicles at most are able to depart from a network per hour, and the critical density corresponding to the network capacity reflects the optimal load of a road network. By comparing MFDs under different network design schemes, the optimal design strategy is determined as the design leading to the maximum network capacity.

$$Q = \max_{k \in K} Q_k \qquad \text{Eq. (21)}$$

s.t.

$$\sum_{a \in \bar{A}} b_a y_a \leq B\,, \qquad \forall a \in \bar{A} \qquad \text{Eq. (22)}$$

$$A = A^0 \cup \{a | y_a > 0\,,\ a \in \bar{A}\} \qquad \text{Eq. (23)}$$

$$Q_k = \frac{\sum_{a \in A} x_a^k \cdot l_a}{\sum_{a \in A} l_a}\,, \qquad \forall k \in K \qquad \text{Eq. (24)}$$

$$y_a = \{0,1\}\,, \qquad \forall a \in \bar{A} \qquad \text{Eq. (25)}$$

In objective function (21), the optimal network capacity is expressed as the maximum weighted flow in all feasible building plans under varied traffic demand scenarios. Constraint (22) ensures the total cost of building new roads not to overrun the given budget. Constraint (23) is used to calculate the extended network A based on original network A^0 and potential links to build. Constraint (24) is a calculation function for weighted flow Q_k. Constraint (25) decides whether or not to construct the new road a.

3.4.2 Lower-level Flow Assignment

Travelers in the lower level are assumed to follow the user equilibrium (UE) principle whose purpose is to minimize their own travel cost described in formula (26). Constraint (27) depicts the OD demand conservation law under each traffic demand scenario, constraint (28) demonstrates the relationship between link flow and route flow under each traffic demand scene, and constraint (29) guarantees the nonnegativity of the route flow.

$$Z^k = \min \sum_{a \in A} \int_0^{x_a^k} t_a^k(x_a^k) dx\,, \quad \forall k \in K \qquad \text{Eq. (26)}$$

s.t.

$$\sum_{p \in P_{rs}} f_{p,k}^{rs} = q_k^{rs}\,, \qquad \forall rs \in D, k \in K \qquad \text{Eq. (27)}$$

$$x_a^k = \sum_{rs \in D} \sum_{p \in P_{rs}} f_{p,k}^{rs} \delta_{a,p}^{rs,k}\,, \qquad \forall a \in A, k \in K \qquad \text{Eq. (28)}$$

$$f_{p,k}^{rs} \geq 0\,, \qquad \forall p \in P_{rs}, rs \in D, k \in K \qquad \text{Eq. (29)}$$

To acquire the link travel time $t_a^k(x_a^k)$ in the objective function (26), the following Bureau of Public Roads (BPR) function is introduced as Equation (30) relating travel time to traffic flow.

$$t_a^k(x_a^k) = t_a^{k,f} \cdot \left[1 + 0.15\left(\frac{x_a^k}{C_a^k}\right)^4\right] \qquad \text{Eq. (30)}$$

Updating traffic network, achieving lower-level UE and producing MFDs are three keys for finding a solution of the proposed model. Usually, network assignment flow can be calculated by solving UE in each feasible network design plan, but both vehicle density and vehicle accumulation of each link can't be acquired. What's more, static UE is hard to produce realistic traffic network state, and is unable to relate to these influencing factors of MFDs: driver behaviours, network load capacity, actual network output, traffic conflict points, traffic composition and road types etc. In view of this, VISSIM is introduced in this report to simulate equilibrium flow under randomly generated OD demands, and further to update traffic network state and output traffic data for plotting MFDs. In VISSIM, to reduce intricate network drawing work, the original network with all candidate links is drawn in advance, and all of the network information (network input, topology and link length) can be extracted to Python console by the COM interface. In Python, network flow assignment is first calculated, and then, according to the assignment results, route decisions are obtained to set up simulation configuration.

In the implementation process, in order to reduce the impact of abnormal data on the model, the highest centroid of clustering results of simulation data in the lower-level UE problem is selected to evaluate the network performance. More specifically, we get data points through weighting the sets (density, flow) from VISSIM output. Given the data points and number of clusters, k-means clustering algorithm is used then to calculate the centroid of each cluster by taking the mean of all data points assigned to that centroid's cluster. By comparing the flow values of all the centroids, the largest flow value is defined as the network capacity.

3.4.3 Solution Algorithm

For clarity, we give Figure 17 to illustrate the algorithmic framework straightforwardly, notations in which are listed in Table 4. As shown, at the beginning of the algorithm, feasible solutions are generated by the budget constraint (22) in the upper level. Each feasible solution represents a link group which can be constructed on the original road network. Every time a new link group is added to the original network, we apply the classic Frank-Wolfe algorithm in the newly generated network to solve the flow assignment model in the lower level, and traffic flow on each link is calculated. Consequently, given link flow, we call the VISSIM COM in Python environment to determine vehicle routes. Through simulating the extended road network, the traffic flow and density for each link can be output and used to calculate the weighted flow and density by weighting the link length. With weighted flow and weighted density at hand, we are able to fit an MFD and extract the maximum weighted flow as the network capacity. To reduce the impact of abnormal data on the result, we use k-means clustering algorithm to get the network capacity.

By comparing with the result in the previous step, a present optimal solution can be determined. If the last link group in the feasible solution set is not reached, a new link group needs to be added to the original network again. The procedure keeps running until the last link group is examined and then the encountered best solution will be reached.

Table 4. Notations and Definitions in Solution Algorithm

Notation	Detailed Definition
G	The original road network drawn in VISSIM
MFD_0	Fitted MFD for the original network G
MFD_Y	Fitted MFD for New_G_Y
MFD_{Y^*}	Global optimal MFD
New_G_Y	An extended network $\{G \cup Y\}$ by adding new link group Y to the original network
Q_0	The maximum weighted flow of MFD_0
Q_Y	The maximum weighted flow of MFD_Y
Q^*	Global maximum weighted flow
$Sim\_interval$	Simulation interval
T	Simulation period
Y	Link group index
Y^*	Global optimal link group index
t	Time index
Φ	The container of candidate link groups satisfying budget constraints

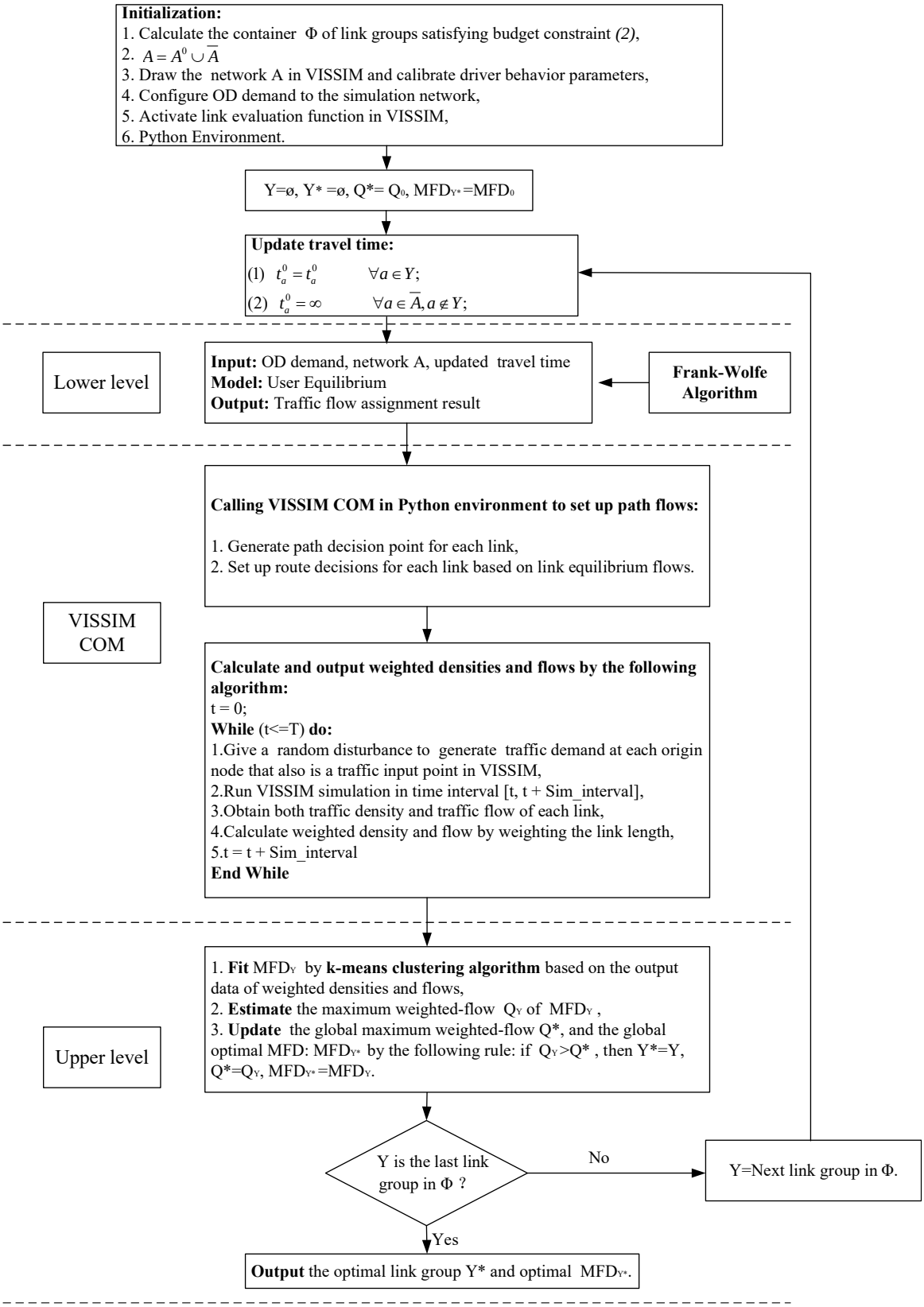

Figure 17. Algorithmic Framework for Solution Strategies.

3.5 RESULTS

To test the proposed methodology, a simulation in VISSIM 10 with COM interface connecting to Python 3.6 is implemented in Sioux Falls network *(50)*. As shown in Figure 18, there are 24 nodes and 76 directed links in the original Sioux Falls network drawn in black solid lines. Each node is both an origin and a destination, so there are total of 552 OD pairs in this network, and the OD demand is half of that in LeBlanc *(50)*.

Now the government plans to build two-way streets in the Sioux Falls network to improve the network operation. In this case study there are 4 pairs of candidate links in $\bar{A}$, respectively (7-16), (9-11), (11-15) and (13-14) drawn in red dashed lines. Each pair of links contains two links in opposite directions, for example, link pair (7-16) includes one link from node 7 to node 16 and one link from node 16 to node 7. Assuming the construction cost of each pair of links is the same, the capital budget can only afford one pair of links to be built.

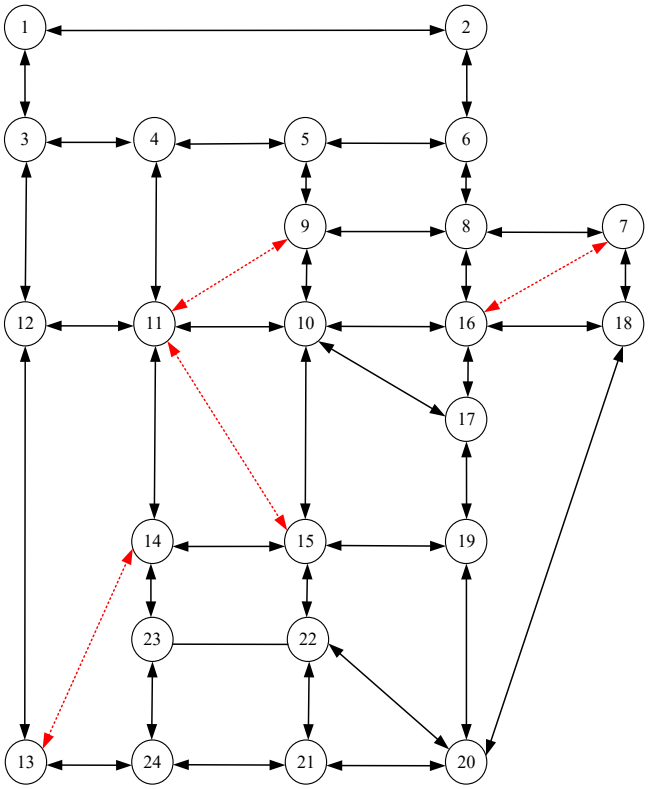

Figure 18. Sioux Falls Test Network.

3.5.1 MFD Results

In order to get the MFD of Sioux Falls network under demand uncertainty, OD demand is changed randomly every 200 seconds ranging from 0 to double the original input, and the simulation time is totally 80,000 seconds (about 22 hours), indicating 400 demand fluctuations in the process of simulation.

During simulation, the traffic flow, density and speed in each link are collected every second. Through weighting both of flow and density with link length every 200 seconds by the following formulas: $q^w = \sum_a q_a l_a / \sum_a l_a$, $d^w = \sum_a d_a l_a / \sum_a l_a$, the MFD curve is made with the weighted network density as abscissa and the space-mean network flow as vertical coordinate. In the formulas, q^w and d^w represent the weighted network flow and weighted network density respectively, l_a is denoted by length of link a, q_a means the flow of link a and d_a stands for the density of link a.

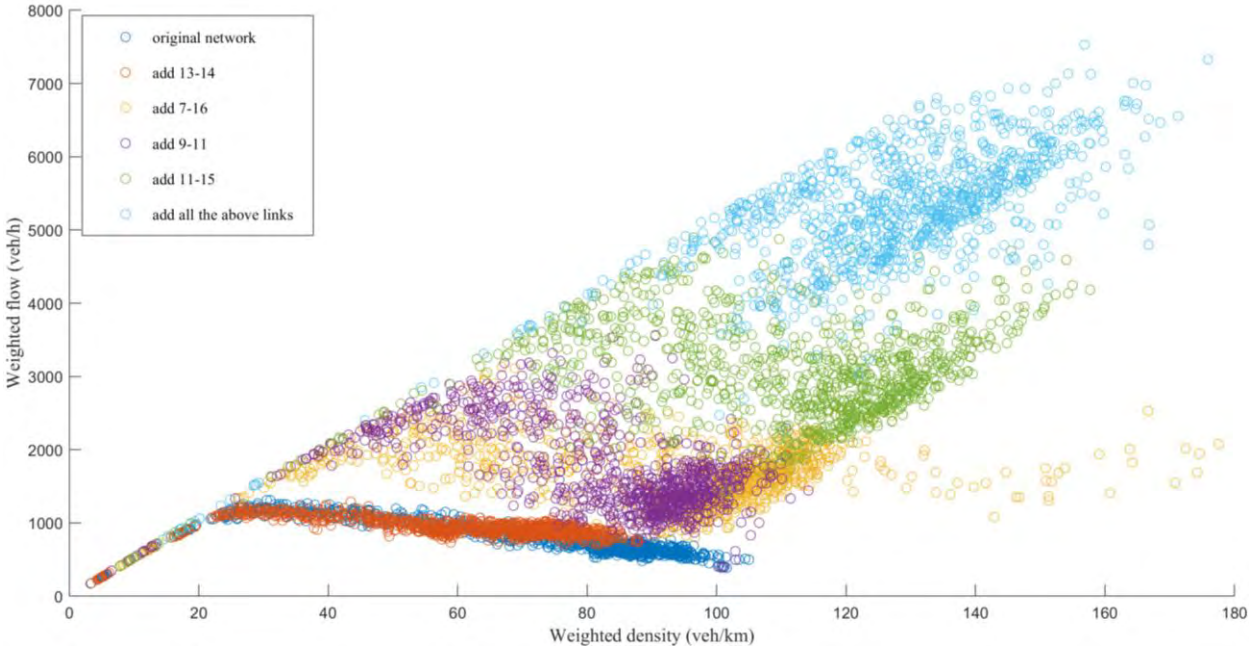

Figure 19. MFDs of Different Extended Sioux Falls Networks.

The MFDs of different extended Sioux Falls networks are plotted in Figure 19, where x-axis and y-axis represent weighted density and space-mean flow respectively. The six scenarios are the original Sioux Falls network and extended networks by adding link pair (13-14), adding link pair (7-16), adding link pair (9-11), adding link pair (11-15) and adding all the candidate link pairs (13-14, 7-16, 9-11, 11-15) in the original Sioux Falls network. Figure 19 illustrates a comparative appraisal of sixed simulated scenarios to demonstrate the change of MFDs before and after constructing different link groups in the Sioux Falls network. We can easily derive that building all the candidate links achieves the most remarkable improvements in network capacity. However, under a certain budget, only one link group is affordable in this case, the addition of link pair (11-15) leads to the maximum performance improvements. To obtain the capacity of each extended network, k-means clustering algorithm is implemented to extract the saturated state of each MFD, and the centroid of saturated state depicts the network capacity, as shown in Figure 20.

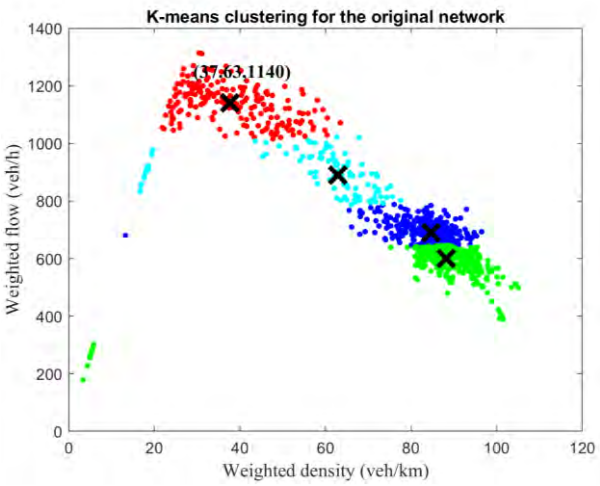
K-means clustering for the original network
(37.63,1140)
Weighted flow (veh/h)
Weighted density (veh/km)

(a)

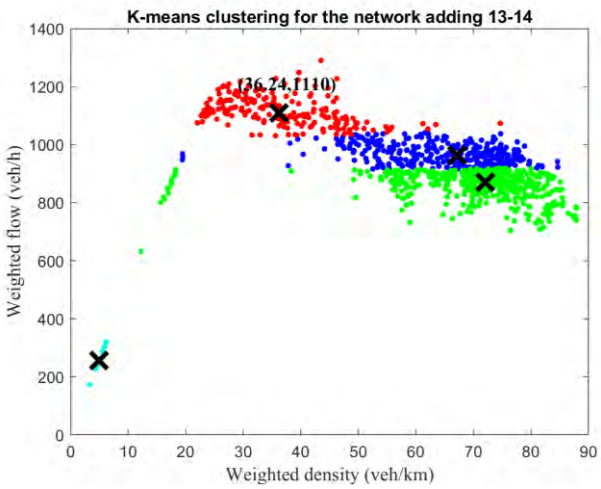
K-means clustering for the network adding 13-14
(36.24,1110)
Weighted flow (veh/h)
Weighted density (veh/km)

(b)

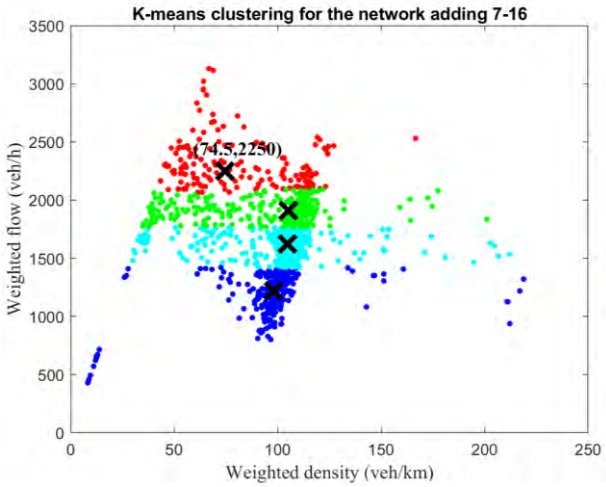
K-means clustering for the network adding 7-16
(74.5,2250)
Weighted flow (veh/h)
Weighted density (veh/km)

(c)

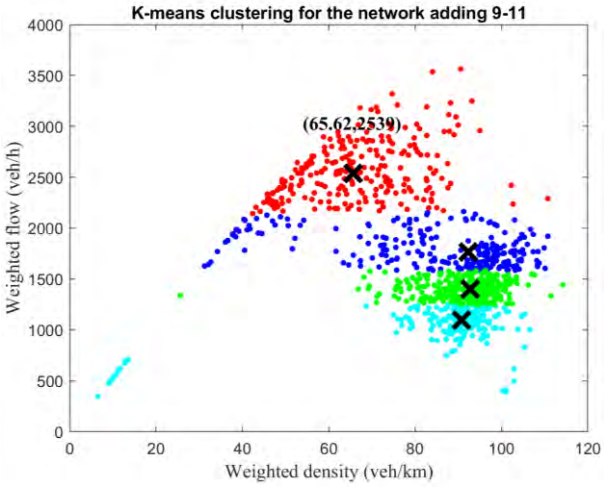
K-means clustering for the network adding 9-11
(65.62,2539)
Weighted flow (veh/h)
Weighted density (veh/km)

(d)

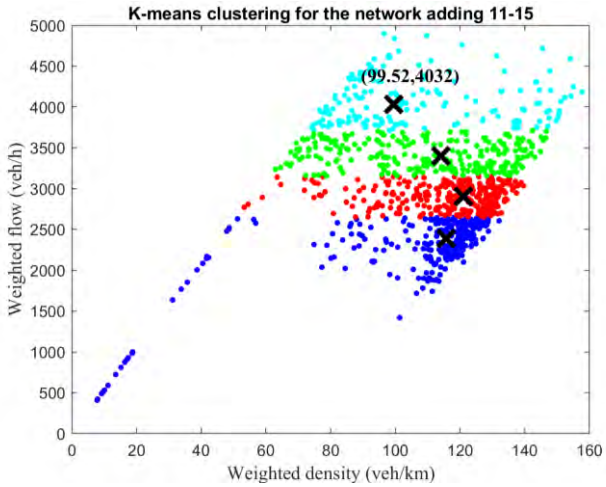
K-means clustering for the network adding 11-15
(99.52,4032)
Weighted flow (veh/h)
Weighted density (veh/km)

(e)

Figure 20. K-means Clustering and Capacities of (a) the original network and Different Extended Sioux Falls Networks by Adding Link Pair (b) 13-14 (c) 7-16 (d) 9-11 (e) 11-15.

Building link pair (11-15) increases the network capacity most, from 1140 veh/h to 4032 veh/h and the corresponding critical density triples from 37.63 veh/km to 99.52 veh/km. That is to say, after building link pair (11-15), not only is the network outflow doubled but also the road network is able to accommodate much more vehicles. When the network density reaches about 90 veh/km, the original Sioux Falls network is almost at a standstill, but the extended network containing links (11-15) operates in an incredibly high throughput. In addition, both link pair (9-11) and (7-16) double the network capacity to 2539 veh/h and 2250 veh/h respectively. However, far from increasing the network flow, the addition of link pair (13-14) reduces the network capacity from 1140 to 1110 veh/h. These results provide an order of priority for the candidate links to be built, which is link group (11-15), (9-11), (7-16), and link pair (13-14) should be avoided.

3.5.2 Capacity Paradox

Figure 20(a) and 20(b) depict the MFDs of the original Sioux Falls network and the extended network that adding link pair (13-14) to the original Sioux Falls network respectively. To our surprise, the network capacity of the original Sioux Falls network is 1140 veh/h, but when we build new links (13-14) to the Sioux Falls network, the network capacity reduces to 1110 veh/h instead. Moreover, the optimal density decreases as well from 36.63 veh/km to 36.24 veh/km. That means, to maintain a network operating in the maximum flow, after building link pair (13-14), fewer vehicles are allowed to travel in the Sioux Falls network.

The above counter-intuitive phenomenon can be explained by the capacity paradox, where the addition of new links to an existing network may worsen the network in terms of reduction in maximum network flow *(56).* The capacity paradox is introduced by Braess paradox *(57),* in which adding a new link will result in a higher cost in a user optimized network. As we have highlighted before, travel time is vulnerable to OD demand, and the occurrence of Braess paradox is no exception. For example, a link adding to the existing road network could increase the network performance when the current demand is relatively low. However, if the future demand increases to a sufficient extent, the same new link may, in contrast, result in longer travel time. Therefore, the result of a travel time-based network design problem is not fit for a network with stochastic demand. Conversely, due to the stable property of MFDs, the solution of an MFD-based network design problem is robust and suited for a long-term design. The proposed methodology also has the ability to avoid capacity paradox, because the objective of this model is to maximize the network capacity.

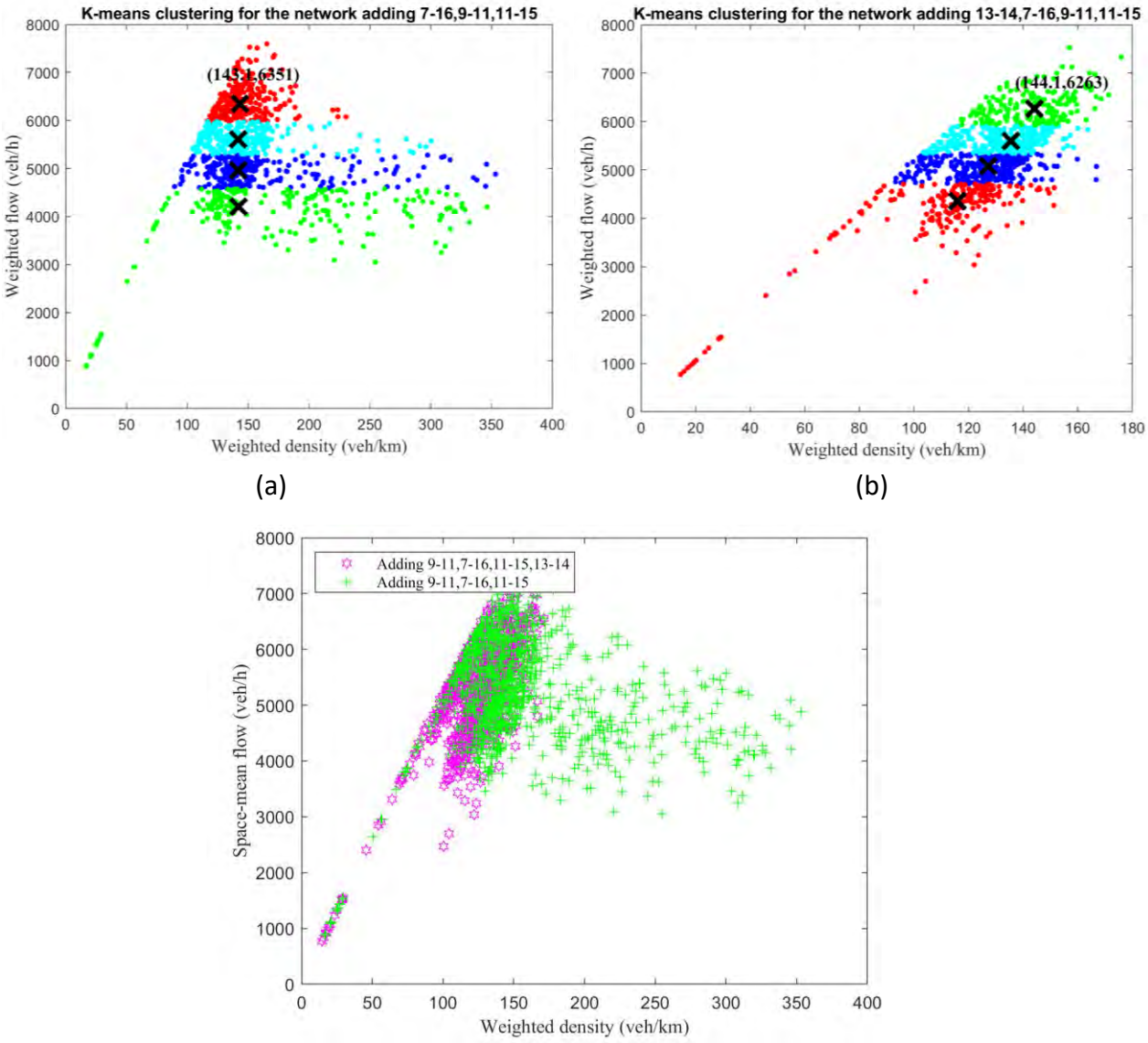

Figure 21. K-means Clustering and Capacities of the Extended Sioux Falls Networks by Adding Link Pairs (a) 7-16,9-11,11-15 (b) 7-16,9-11,11-15,13-14 and (c) MFD Comparison between the Two Extended Sioux Falls Networks.

Moreover, Figures 21(a) and 21(b) show MFDs of two extended Sioux Falls networks. The network adding three link pairs achieves a better performance than the network adding four link pairs, especially when traffic is in the congested condition. To be specific, magenta dots describe how the space-mean flow in the extended Sioux Falls network, after the addition of link pairs (9-11,7-16,11-15,13-14), evolves as the weighted density increases. It is noteworthy that, once the density approaches about 150 veh/km, no more vehicles are allowed to enter the network. Traffic congestion spreads quickly, both of the density and flow would experience a sudden drop, eventually forming a traffic standstill. The phenomenon is called clockwise hysteresis loop *(58).*

According to Geroliminis and Sun *(46,59),* the hysteresis phenomenon in the network level happens because of different degrees of spatial heterogeneity in vehicle density in the onset and offset of the peak period. However, the hysteresis phenomenon disappears in the Sioux Falls network extended by adding only three link pairs (7-16,9-11,11-15). As shown by the green dots in Figure 21(c), after the weighted density is 150 veh/km, although the network flow gradually decreases, more vehicles are allowed to pour into the network. It is verified again that building more roads is not always better, the selection of roads to be built need to be careful.

3.6 CONCLUSION

This chapter has outlined a novel approach to the measurement of network performance with respect to the network capacity and developed a bi-level programming model for the formulation of the DNDP. Following are the main contributions of this chapter: 1) Different from the existing traditional models for DNDPs, this model aims to improve the network performance by obtaining the optimal MFD-based network capacity. The proposed method is appropriate for deciding which links should be built when traffic demand is stochastic. 2) To solve the proposed model, an algorithm based on microsimulation software VISSIM is designed, and the output MFDs are guaranteed to incorporate complicated driver behaviours and random demand scenarios simultaneously. 3) Results in the case study have showed effectiveness of the proposed methodology based on MFD in solving DNDPs under stochastic demands. For the test network, candidate link pair (11-15) is given the highest priority because it improves the network performance most, tripling the network capacity. 4) Interestingly, capacity paradox occurs in the test network, where building a new link reduces the network capacity, even incurs a hysteresis loop. The proposed approach has the ability to avoid the capacity paradox, because pursing a new network with higher capacity is the objective of this research.

3.7 RECOMMENDATIONS

There are still limitations in the proffered network design for the inability to address upheaval of demand in a methodologically sound manner, because rapidly changing traffic demands drastically affect MFD shape. Therefore, this MFD-based programming model may be infeasible for demand surge or slump situations. Besides, spatial distribution of vehicle density in the network is a determinant that affects the scatter of an MFD and its shape *(46).* A large scale heterogeneous network with uneven distribution of congestion may not have a well-defined MFD, thus the proposed methodology cannot be directly applied to an inhomogeneous network unless a large scale heterogeneous urban traffic network is partitioned into homogeneous sub-networks.

TECHNOLOGY TRANSFER/IMPLEMENTATION

One work was presented in STRIDE Center's Research Poster Showcase, held during the University of Florida Transportation Institute's (UFTI) reception in Washington D.C. on January

14, 2019, from 5:30 pm to 7:30 pm. Dozens of practitioners, agency personnel, or academics attended the session.

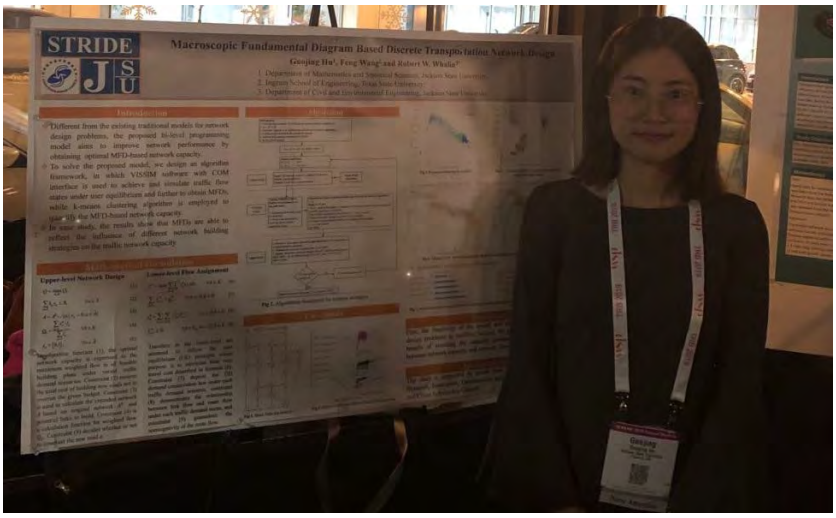

The researcher attending the 2019 UFTI reception in Washington DC

Another work was presented in the student poster session at 2019 Automated Vehicles Symposium (AVS) in Orlando on July 16, 2019, from 5:30 pm to 7:00 pm. Nearly 10 practitioners, agency personnel, and academics discussed with the researchers.

The PI attending the 2019 AVS in Orlando

In addition, two of three related academic papers have been published in journals for disseminating the research outcomes. Besides, the research team plans to hold an online webinar on July 1, 2020 to spread the research findings, benefiting both the scientific community and traffic operators who are responsible for shaping the future of connected and autonomous vehicles.

REFERENCE LIST

1. Truong, L.T., De Gruyter, C., Currie, G. and Delbosc, A., 2017. Estimating the trip generation impacts of autonomous vehicles on car travel in Victoria, Australia. *Transportation*, *44*(6), pp.1279-1292.
2. Zhao, Y. and Kockelman, K.M., 2018. Anticipating the regional impacts of connected and automated vehicle travel in Austin, Texas. *Journal of Urban Planning and Development*, *144*(4), p.04018032.
3. Chen, D., Ahn, S., Chitturi, M. and Noyce, D.A., 2017. Towards vehicle automation: Roadway capacity formulation for traffic mixed with regular and automated vehicles. *Transportation research part B: methodological*, *100*, pp.196-221.
4. Talebpour, A., Mahmassani, H.S. and Elfar, A., 2017. Investigating the effects of reserved lanes for autonomous vehicles on congestion and travel time reliability. *Transportation Research Record*, *2622*(1), pp.1-12.
5. Ye, L. and Yamamoto, T., 2018. Impact of dedicated lanes for connected and autonomous vehicle on traffic flow throughput. *Physica A: Statistical Mechanics and its Applications*, *512*, pp.588-597.
6. Harwood, N., and Reed, N., 2014. Modelling the impact of platooning on motorway capacity. *Road Transport Information and Control Conference*.
7. Treiber, M., Hennecke, A. and Helbing, D., 2000. Congested traffic states in empirical observations and microscopic simulations. *Physical review E*, *62*(2), p.1805.
8. Derbel, O., Peter, T., Zebiri, H., Mourllion, B. and Basset, M., 2013. Modified intelligent driver model for driver safety and traffic stability improvement. *IFAC Proceedings Volumes*, *46*(21), pp.744-749.
9. Dey, K.C., Yan, L., Wang, X., Wang, Y., Shen, H., Chowdhury, M., Yu, L., Qiu, C. and Soundararaj, V., 2015. A review of communication, driver characteristics, and controls aspects of cooperative adaptive cruise control (CACC). *IEEE Transactions on Intelligent Transportation Systems*, *17*(2), pp.491-509.
10. Zhao, L. and Sun, J., 2013. Simulation framework for vehicle platooning and car-following behaviors under connected-vehicle environment. *Procedia-Social and Behavioral Sciences*, *96*, pp.914-924.
11. Mahmassani, H.S., 2016. 50th anniversary invited article—autonomous vehicles and connected vehicle systems: Flow and operations considerations. *Transportation Science*, *50*(4), pp.1140-1162.
12. Talebpour, A. and Mahmassani, H.S., 2016. Influence of connected and autonomous vehicles on traffic flow stability and throughput. *Transportation Research Part C: Emerging Technologies*, *71*, pp.143-163.

13. Schakel, W.J., Van Arem, B. and Netten, B.D., 2010, September. Effects of cooperative adaptive cruise control on traffic flow stability. In *13th International IEEE Conference on Intelligent Transportation Systems* (pp. 759-764). IEEE.
14. Talebpour, A., Mahmassani, H.S. and Hamdar, S.H., 2015. Modeling lane-changing behavior in a connected environment: A game theory approach. *Transportation Research Part C: Emerging Technologies*, *59*, pp.216-232.
15. Ghiasi, A., Hussain, O., Qian, Z.S. and Li, X., 2017. A mixed traffic capacity analysis and lane management model for connected automated vehicles: A Markov chain method. *Transportation Research Part B: Methodological*, *106*, pp.266-292.
16. Shi, Y., He, Q. and Huang, Z., 2019. Capacity analysis and cooperative lane changing for connected and automated vehicles: Entropy-based assessment method. *Transportation research record*, *2673*(8), pp.485-498.
17. Liu, H., Kan, X.D., Shladover, S.E., Lu, X.Y. and Ferlis, R.E., 2018. Modeling impacts of cooperative adaptive cruise control on mixed traffic flow in multi-lane freeway facilities. *Transportation Research Part C: Emerging Technologies*, *95*, pp.261-279.
18. Zhou, M., Qu, X. and Jin, S., 2016. On the impact of cooperative autonomous vehicles in improving freeway merging: a modified intelligent driver model-based approach. *IEEE Transactions on Intelligent Transportation Systems*, *18*(6), pp.1422-1428.
19. PTV AG, VISSIM 5.20 User Manual. Karlsruhe, Germany. 2009, pp. 130-133.
20. Tettamanti, T. and Horváth, M.T., 2020. A practical manual for Vissim-COM programming in Matlab 4th edition for Vissim version 2020.
21. Aghabayk, K., Sarvi, M., Young, W. and Kautzsch, L., 2013, October. A novel methodology for evolutionary calibration of Vissim by multi-threading. In *Australasian Transport Research Forum*, *36*(1), pp. 1-15.
22. Songchitruksa, P., Bibeka, A., Lin, L.I. and Zhang, Y., 2016. Incorporating driver behaviors into connected and automated vehicle simulation (No. ATLAS-2016-13). Center for Advancing Transportation Leadership and Safety (ATLAS Center).
23. Beza, A.D. and Zefreh, M.M., 2019. Potential Effects of Automated Vehicles on Road Transportation: A Literature Review. *Transport and Telecommunication Journal*, *20*(3), pp.269-278.
24. Atkins, 2016. Research on the Impacts of Connected and Autonomous Vehicles (CAVs) on Traffic Flow. *Department for Transport*. (SO13994/3).
25. Ye, L. and Yamamoto, T., 2018. Modeling connected and autonomous vehicles in heterogeneous traffic flow. *Physica A: Statistical Mechanics and its Applications*, *490*, pp.269-277.
26. Levin, M.W. and Boyles, S.D., 2016. A multiclass cell transmission model for shared human and autonomous vehicle roads. *Transportation Research Part C: Emerging Technologies*, *62*, pp.103-116.

27. Qin, Y. and Wang, H., 2019. Cell Transmission Model for Mixed Traffic Flow with Connected and Autonomous Vehicles. *Journal of Transportation Engineering, Part A: Systems*, *145*(5), p.04019014.
28. Amoozadeh, M., Deng, H., Chuah, C.N., Zhang, H.M. and Ghosal, D., 2015. Platoon management with cooperative adaptive cruise control enabled by VANET. *Vehicular communications*, *2*(2), pp.110-123.
29. Olia, A., Razavi, S., Abdulhai, B. and Abdelgawad, H., 2018. Traffic capacity implications of automated vehicles mixed with regular vehicles. *Journal of Intelligent Transportation Systems*, *22*(3), pp.244-262.
30. Tilg, G., Yang, K. and Menendez, M., 2018. Evaluating the effects of automated vehicle technology on the capacity of freeway weaving sections. *Transportation Research Part C: Emerging Technologies, 96*, pp.3-21.
31. Geroliminis, N. and Daganzo, C.F., 2008. Existence of urban-scale macroscopic fundamental diagrams: Some experimental findings. *Transportation Research Part B: Methodological*, *42*(9), pp.759-770.
32. Zhang, L., Garoni, T.M. and de Gier, J., 2013. A comparative study of macroscopic fundamental diagrams of arterial road networks governed by adaptive traffic signal systems. *Transportation Research Part B: Methodological*, *49*, pp.1-23.
33. Yildirimoglu, M., Ramezani, M. and Geroliminis, N., 2015. Equilibrium analysis and route guidance in large-scale networks with MFD dynamics. *Transportation Research Procedia*, *9*, pp.185-204.
34. Mittal, A., Mahmassani, H.S. and Talebpour, A., 2017. Network flow relations and travel time reliability in a connected environment. *Transportation Research Record*, *2622*(1), pp.24-37.
35. Buisson, C. and Ladier, C., 2009. Exploring the impact of homogeneity of traffic measurements on the existence of macroscopic fundamental diagrams. *Transportation Research Record*, *2124*(1), pp.127-136.
36. Tsubota, T., Bhaskar, A. and Chung, E., 2014. Macroscopic fundamental diagram for Brisbane, Australia: empirical findings on network partitioning and incident detection. *Transportation Research Record*, *2421*(1), pp.12-21.
37. Loder, A., Ambühl, L., Menendez, M. and Axhausen, K.W., 2017. Empirics of multi-modal traffic networks–Using the 3D macroscopic fundamental diagram. *Transportation Research Part C: Emerging Technologies*, *82*, pp.88-101.
38. Ji, Y., Daamen, W., Hoogendoorn, S., Hoogendoorn-Lanser, S. and Qian, X., 2010. Investigating the shape of the macroscopic fundamental diagram using simulation data. *Transportation Research Record*, *2161*(1), pp.40-48.

39. Daganzo, C.F. and Geroliminis, N., 2008. An analytical approximation for the macroscopic fundamental diagram of urban traffic. *Transportation Research Part B: Methodological*, *42*(9), pp.771-781.
40. Laval, J.A. and Castrillón, F., 2015. Stochastic approximations for the macroscopic fundamental diagram of urban networks. *Transportation Research Procedia*, *7*, pp.615-630.
41. Daganzo, C.F. and Lehe, L.J., 2016. Traffic flow on signalized streets. *Transportation Research Part B: Methodological*, *90*, pp.56-69.
42. Tilg, G., Amini, S. and Busch, F., 2019. Arterial Macroscopic Fundamental Diagram: A Comparison of Analytical Approximations and Empirical Data from Munich. *In 98th Annual Meeting of the Transportation Research Board (TRB 2019).*
43. Newell, G.F., 1993. A simplified theory of kinematic waves in highway traffic, part II: Queueing at freeway bottlenecks. *Transportation Research Part B: Methodological*, *27*(4), pp.289-303.
44. Sala, M. and Soriguera, F., 2020. Macroscopic Modeling of Connected Autonomous Vehicle Platoons under Mixed Traffic Conditions. *Transportation Research Procedia*, 47, pp.163-170.
45. Lighthill, M.J. and Whitham, G.B., 1955. On kinematic waves II. A theory of traffic flow on long crowded roads. *Proceedings of the Royal Society of London. Series A. Mathematical and Physical Sciences*, *229*(1178), pp.317-345.
46. Geroliminis, N., and J. Sun, 2011. Properties of A Well-Defined Macroscopic Fundamental Diagram. *Transportation Research Part B*, *45*(3), pp.605-617.
47. Ramezani, M., J.Haddad, and N. Geroliminis, 2015. Dynamics of Heterogeneity in Urban Networks: Aggregated Traffic Modeling and Hierarchical Control. *Transportation Research Part B: Methodological*, *74*, pp.1-19.
48. Di, Z., Yang, L., Qi, J. and Gao, Z., 2018. Transportation network design for maximizing flow-based accessibility. *Transportation Research Part B: Methodological*, *110*, pp.209-238.
49. Geroliminis, N. and Daganzo, C.F., 2007, January. Macroscopic modeling of traffic in cities. In *Transportation Research Board 86th Annual Meeting* (No. 07-0413). No. 07-0413.
50. Leblanc, L.J., 1975. An algorithm for the discrete network design problem. *Transportation Science*, *9*(3), pp.183-199.
51. Behbahani, H., Nazari, S., Kang, M.J. and Litman, T., 2019. A conceptual framework to formulate transportation network design problem considering social equity criteria. *Transportation research part A: policy and practice*, *125*, pp.171-183.
52. Jiang, Y. and Szeto, W.Y., 2015. Time-dependent transportation network design that considers health cost. *Transportmetrica A: transport science*, *11*(1), pp.74-101.

53. Yang, H. and Wang, J.Y., 2002. Travel time minimization versus reserve capacity maximization in the network design problem. *Transportation Research Record*, *1783*(1), pp.17-26.
54. Miandoabchi, E., Daneshzand, F., Szeto, W.Y. and Farahani, R.Z., 2013. Multi-objective discrete urban road network design. *Computers & Operations Research*, *40*(10), pp.2429-2449.
55. Mazloumian, A., Geroliminis, N. and Helbing, D., 2010. The spatial variability of vehicle densities as determinant of urban network capacity. *Philosophical Transactions of the Royal Society A: Mathematical, Physical and Engineering Sciences*, *368*(1928), pp.4627-4647.
56. Yang, H. and Bell, M.G., 1998. A capacity paradox in network design and how to avoid it. *Transportation Research Part A: Policy and Practice*, *32*(7), pp.539-545.
57. Braess, D., 1968. Über ein Paradoxon aus der Verkehrsplanung. *Unternehmensforschung*, *12*(1), pp.258-268.
58. Gayah, V.V. and Daganzo, C.F., 2011. Clockwise hysteresis loops in the macroscopic fundamental diagram: an effect of network instability. *Transportation Research Part B: Methodological*, *45*(4), pp.643-655.
59. Geroliminis, N. and Sun, J., 2011. Hysteresis phenomena of a macroscopic fundamental diagram in freeway networks. *Procedia-Social and Behavioral Sciences*, *17*, pp.213-228.

APPENDIX

Abbreviations

CAV- autonomous and connected vehicle

HV- human-driven vehicle

IDM- intelligent driver model

ACC- adaptive cruise control

CACC- cooperative adaptive cruise control

V2V- vehicle-to-vehicle

FD- fundamental diagram

MFD- macroscopic fundamental diagram

CV- connected vehicle

MC- method of cut

SA- stochastic approximation

LP- linear program

SSE- sum of squared errors

NDP- network design problem

CNDP- continuous network design problem

DNDP- discrete network design problem

MNDP- mixed network design problem

OD- origin-destination

UE- user equilibrium